EXTREME HURRICANE SURGE ESTIMATION

FOR TEXAS COASTAL BRIDGES

USING DIMENSIONLESS SURGE RESPONSE FUNCTIONS

A Thesis

by

YOUN KYUNG SONG

Submitted to the Office of Graduate Studies of
Texas A&M University
in partial fulfillment of the requirements for the degree of

MASTER OF SCIENCE

August 2009

Major Subject: Civil Engineering

EXTREME HURRICANE SURGE ESTIMATION

FOR TEXAS COASTAL BRIDGES

USING DIMENSIONLESS SURGE RESPONSE FUNCTIONS

A Thesis

by

YOUN KYUNG SONG

Submitted to the Office of Graduate Studies of
Texas A&M University
in partial fulfillment of the requirements for the degree of

MASTER OF SCIENCE

Approved by:

Co-Chairs of Committee,	Kuang-An Chang
	Jennifer L. Irish
Committee Members,	David Brooks
Head of Department,	David V. Rosowsky

August 2009

Major Subject: Civil Engineering

ABSTRACT

Extreme Hurricane Surge Estimation for Texas Coastal Bridges

Using Dimensionless Surge Response Functions. (August 2009)

Youn Kyung Song, B.S., Han Yang University

Co-Chairs of Advisory Committee: Dr.Kuang-An Chang
Dr. Jennifer L. Irish

Since the devastating hurricane seasons of 2004, 2005, and 2008, the stability and serviceability of coastal bridges during and following hurricane events have become a main public concern. Twenty coastal bridges, critical for hurricane evacuation and recovery efforts, in Texas have been identified as vulnerable to hurricane surge and wave action. To accurately assess extreme surges at these bridges, a dimensionless surge response function methodology was adopted. The surge response function defines maximum surge in terms of hurricane meteorological parameters such as hurricane size, intensity, and landfall location. The advantage of this approach is that, given a limited set of discrete hurricane surge data (either observed or simulated), all possible hurricane surges within the meteorological parameter space may be described. In this thesis, we will first present development of the surge response function methodology optimized to include the influence of regional continental shelf geometry. We will then demonstrate surge response function skill for surge prediction by comparing results with surge observations for Hurricanes Carla (1961) and Ike (2008) at several stations along the

coast. Finally, we apply the improved surge response function methodology to quantify extreme surges for Texas coastal bridge probability and vulnerability assessment.

ACKNOWLEDGEMENTS

First, I would like to express my gratitude to my committee chairs, Dr. Kuang-An Chang and Dr. Jennifer Irish. Most of all, they have taught me the correct attitude as a graduate student. Dr. Chang has provided me with full support from the beginning of my graduate studies, including opportunities to work with people from various academic and professional fields. While carrying out the work to accomplish this research project with him, Dr. Chang instilled in me the importance of being confident about what I am doing through ceaseless preparation and study. Dr. Irish has always encouraged me to make full use of the textbook principles and harmonize with the engineering judgment when solving the real world problems. I believe her progressive spirit and assiduity reflected in her leadership will remain as an inspiring action in my future life as a researcher. I would also like to extend my sincere thank to members of committee, Dr. David Brooks and Dr. Billy Edge for their instructive advice and constructive concern at every step of this research work. Having them as advisers and consultants was always encouraging and kept me stimulated. This research was funded by the Texas Department of Transportation. I want to thank them for their financial and systematic support for the last two years' research activities. In addition, I would like to extend thanks to all of my fellow graduate students at Texas A&M University and friends back in my hometown. Finally, I want to thank to my respected parents, Chang-ho Song and Hee-sun Jung, my brave sister, Yoon-jung Song, and my lovely brother Min-soo Song, for their earnest support and unfailing love.

TABLE OF CONTENTS

CHAPTER Page

LIST OF FIGURES

Page

Page

LIST OF TABLES

Page

CHAPTER I

INTRODUCTION:

STORM SURGE ESTIMATION NEAR TEXAS COASTAL BRIDGES

Damage to hurricanes striking in 2004, 2005, and 2007 to the present have called public attention to the importance of accurate assessment of hurricane impacts on coastal residents and structures. Especially, the stability and serviceability of coastal bridges directly exposed to intensified wave forces during hurricane events have become a main concern. There are a great number of coastal highways and bridges distributed throughout the entire Texas coast along the Gulf of Mexico. After inspection of the geography and landscape of their locations, twenty coastal bridges closely associated with the life of nearby communities, especially during hurricane evacuation, were suspected to be vulnerable to hurricane flooding. As a means for more concrete quantification and reliable estimation, a Surge Response Function methodology (Irish et al., 2009) was adopted.

A Surge Response Function (SRF, Irish et al., 2009) is a parametric representation of the continuous surge response surface in a dimensionless form. Based on the joint probability method with optimal sampling (JPM-OS), the surge response function approach (Resio et al., 2009) suggested that a maximum surge surface (ζ) could

---

This thesis follows the style of *the Journal of Waterway, Port, Coastal and Ocean Engineering.*

be described by a number of major hurricane parameters such as hurricane size, intensity, track angle, forward speed, and the relative distance to hurricane landfall location. Furthermore, the physical relationship between the maximum surge and relevant hurricane parameters was identified and used to develop the scaled parameters characterizing spatial extent of surge (x') and hurricane surge (ζ '). These physical laws introduced in the surge response function method (Irish et al., 2009) is beneficial since it has a potential for more reliable surge estimation since the derived dimensionless parameters allow a better interpolation for the tracks lying between the tracks where the numerical simulation data is available.

For evaluating hurricane impact on the selected 20 coastal bridges widely spread out throughout the Texas coast, numerical hurricane surge simulations for 15 parallel tracks entering to the Gulf of Mexico following northeasterly path were carried out. During the course of this work to determine the surge response functions at the selected bridge regions, however, a notable shifting in the location of dimensionless peak surge – the highest surge possible among all studied storm surges at a given location - has been found for those bridges located away from Matagorda Bay with respect to Matagorda Bay results studied by Irish et al. (2009) Also, more prominent scatter in the surge data for these storms to right of the hurricane landfall location have been found in data distribution at the coastal stations nearby Galveston Bay. After investigation into the regional characteristics, it was found that the continental shelf width –defined here as the off-shore distance from the coastline to the 30m water depth - near the Galveston coast changes more rapidly and is much wider than those at other regions to the south.

Therefore, the effect of relative storm size with respect to the continental shelf width was investigated in order to improve SRF performance.

Based on these new findings, in this study we have made a number of modifications to improve the initial surge response function so it can be applicable for all 20-target bridges over a range of geographical and hurricane meteorological parameters. First, we related the continental shelf width to the continental shelf parameter, λ, so the variance of bottom slope, or the area on which the storm surge is developing, is considered when predicting the peak surge location.

The objective of this study is to evaluate hurricane impact on Texas coastal bridges by optimizing the use of a SRF. In chapter 1, the overview of the previous studies related to the theories and principles behind the SRF approach is presented. In chapter 2, the selection of twenty Texas coastal bridges vulnerable to hurricane flooding is displayed along with their locations along the Texas coast. In CHAPTER III, a course of work to determine SRFs at a given coastal region will be demonstrated. For validation, the defined SRFs will be applied to quantify storm surge levels at several stations in Matagorda Bay and Galveston, and the prediction will be compared to High Water Marks (HWM) and water level gauge data recorded during hurricanes Carla (1961) and Ike (2008), respectively. Finally, discussion on more accurate surge prediction and more efficient use of available data will be presented. Through this thesis, one is expected to obtain more concrete ideas on how the SRF is applied for hurricane impact assessment in real-world application.

CHAPTER II

BACKGROUND AND LITERATURE REVIEW

2.1 Damages to Coastal Bridges due to Storm Surges

A storm surge is a drastic surface sea level rise caused by extreme wind and barometric pressure deficit, among other factors induced by tropical or extratropical cyclones. Aside from the direct loss of lives due to flooding, a sudden rise in the surface water level during recent hurricane seasons brought about serious damages to properties and infrastructure in coastal areas. In the United States, around 53% of the population lives near the coast, and since 1970 there have been 2000 homes per day erected in coastal areas (UN Atlas of the Oceans, 2000). Within the Atlantic or Gulf of Mexico alone, there are more than 25.6 million people in 290,000 km of coastal land area and, more than 96,560 km of roadways are in the 100- year coastal flood plain in the United States (Douglass et al., 2005).

Many hurricane reports evidenced this intrusion of flooded water was the cause of severe damages to coastal highways and bridges along the Gulf of Mexico. For examples, Hurricane Ivan (2004) ravaged the Escambia Bay Bridge and resulted in suspension of traffic and blockage of the supply route. When Hurricane Katrina (2005) attacked the vital coastal bridges along the Gulf coast including the one on the US-90 in Mississippi (Fig. 1), extensive repair at public expense was required. For example;

- $803 million for the bridge deck lifting project for the I-10 Twin Span Bridge in Louisiana

- $226.8 million for the bridge replacement project for the Bay St. Louis bridge on U.S. 90 in Mississippi

In total, $2.75 billion in supplemental appropriation was awarded for the Federal Highway Administration's "Emergency Relief Program" (Collins 2006). Following Hurricane Ike in 2008, the state and interstate highways along the Galveston coast, including SH 87 from the Bolivar Ferry Landing to SH 124 and IH 45-Gulf Freeway (Fig. 2) were closed due to damage and debris on the road and resulted in a $20 million effort for repair (Public Information Office of Texas Department of Transportation 2008).

Fig. 1 Highway 90 bridge damaged during Hurricane Katrina. The bridge was located on US-90 in Biloxi and Gulfport, Mississippi Gulf Coast (From Gulf Coast Information System (GCIS, 2006)

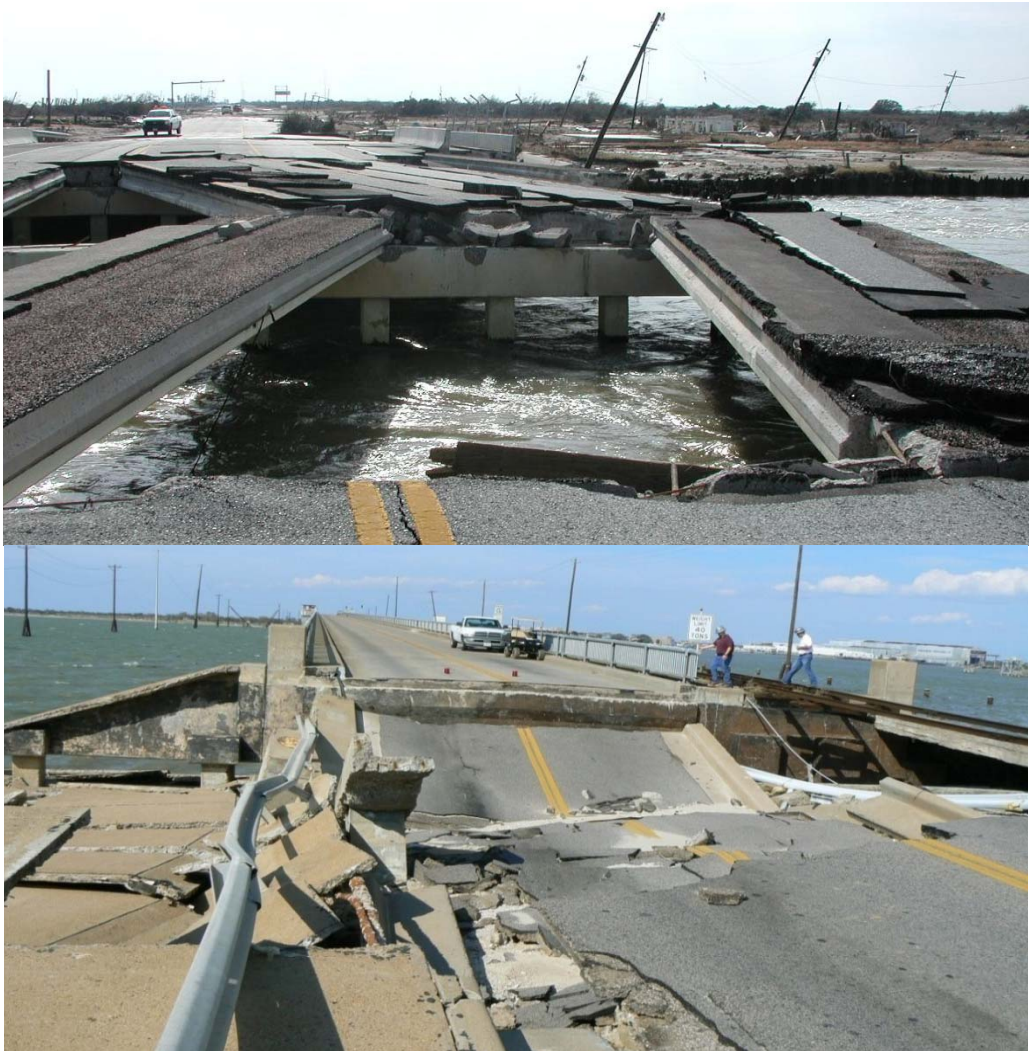

Fig. 2 Two bridges damaged during Hurricane Ike. Rollover Pass located between the communities of Gilchrist and Caplen (top), and Pelican Island Bridge along 51st Street over the Galveston Ship Channel (bottom). (photos courtesy of Dr. Jun Jin (2008), Texas A&M University)

Padgett et al. (2008) have analyzed bridge damage mechanisms based on observations of 44 damaged bridges in Alabama, Louisiana, and Mississippi during Hurricane Katrina. According to their study, major bridge damages during hurricane

events are attributed to the increased uplifting loads and impacts from debris and objects near the bridge, induced by the storm surges, and partially by high winds, scour, and malfunction of electrical and mechanical equipment due to water inundation. Furthermore, the overall analysis showed that the bridges with spans of the same or lower elevation than peak surge levels had experienced severe structural failure during hurricane events. For studies mainly focused on water surface response to hurricane forcing, the wave setup is estimated at about 15% of the total flood level (Irish and Cañizares, 2009). Therefore, in order to examine the stability of the coastal bridges in response to the storm surges, the value of 15% higher than the peak surge levels should be an adequate approximation for this study.

2.2 Governing Equation for Storm Surge

Storm surge levels are determined by both the hurricane meteorological conditions and the geometric characteristics of the coastal regions. The early surge prediction was highly dependent on the historical surge observations (Resio and Westerink, 2008). However, the length of the most surge data was too short and regional extent where the data was recorded was not wide enough to adequately characterize regional geometric factors. Therefore, the reliance on such limited historical data alone resulted in inaccurate characterization of surge responses to the extreme storms. Consequently, in an attempt to make more accurate surge predictions that overcome the existing data limit, researchers' effort for surge predictions focused on developing physics-based hurricane models.

A storm surge is a sea level rise caused by wind stress and low pressure, among other factors, and can be described by the three dimensional equations of mass and momentum. However, we can limit our interest to shallow water hydrodynamic circulation on the regions where the horizontal scale of fluid motion is much larger than the water depth. That is, assuming the horizontal fluid dynamics are more dominant compared to relatively static vertical motion of the flow in the shallow water body, and the water density is constant over the depth, the three dimensional equation of motion and momentum can be vertically integrated to become the two-dimensional shallow water equations (Lynch and Gray, 1979). Therefore, the conservation of mass becomes

$$\frac{\partial H}{\partial t} + \nabla_h (H\vec{u}) = 0 \tag{2.1}$$

The conservation of momentum becomes

$$\frac{\partial \vec{u}}{\partial t} + (\vec{u} \cdot \nabla_h)\vec{u} + g\nabla_h \zeta + f\,\hat{k} \times \vec{u} + \tau_b \vec{u} = \psi \tag{2.2}$$

where
H is total fluid depth,
u is a vertically averaged horizontal velocity,
ζ the is elevation above the mean sea level,
f is the Coriolis parameter,
τ_b is a bottom stress parameter,
$\tilde{N}_h$ is the horizontal gradient operator, and
$\hat{k}$ is the vertical unit vector,
ψ is a forcing term.

Under hurricane forcing, ψ can be represented by the combined effect of atmospheric pressure variations ($\Delta P = P_f - P_c$) between the surface pressure at periphery, P_f and lowest surface pressure, P_c of the storm, surface wind stress (τ_s), and other forces (e.g. wave radiatio stress and tides). The wind stress is empirically defined (Dean and Dalrymple, 2002) as a function of air density (ρ_a), a surface friction coefficient (C_f), and wind speed (U) as

$$\tau_s = \rho_a C_f U^2 \tag{2.3}$$

A setup of surface water in the deep ocean is dominated by pressure deficit due to the low atmospheric pressure at the center of a storm. Storm surge induced by the pressure deficit can be evaluated (Dean and Dalrymple, 2002) by

$$\zeta_B = \frac{\Delta P}{\gamma} \tag{2.4}$$

where
ζ_B is a setup of the surface water due to thebarometric pressure deficit ΔP, and
γ is the specific weight of the water.

On the other hand, storm surge generation at the coast involves more complex interactions between coastal geometry, bathymetry, and wind and pressure forcing. A linearized, steady-state storm surge on the coast can be simplified as (Resio and Westerink, 2008)

$$\zeta_c = \left(\frac{\tau}{gh} \right) W \tag{2.5}$$

where
ζ_c is storm surge at the coast,
τ is hurricane induced wind and barometric stress,
h is a depth of the water,
W is a continental shelf width,
g is the gravitational acceleration.

The close relationship between coastal surges and the geometric factors termed as water depth (h) and shelf width (W) implies that of capturing of the site-dependent characteristics has a make significant impact on the accuracy of surge prediction.

Besides the two components previously mentioned, other mechanisms involved in storm surge generation are momentum transfer due to wave breaking, Coriolis acceleration, astronomical tide forcing, and the reminder of the bottom friction after balanced with the surface wind stress.

2.3 Numerical Studies of Storm Surge Simulations

Considering the heavy reliance of this study on numerical storm simulation results, it is critical to utilize an adequate numerical model that provides sufficient accuracy in prediction. The performance of numerical models to solve shallow water surge problems are documented through many years of careful studies (Lynch, 1983; Westerink and Gray, 1991).

Surge analysis by Westerink et al. (1992 and 1994) investigated the effect of the domain size on the accuracy proved that using the largest East Coast domain encompassing the Western North Atlantic Ocean, the Caribbean Sea, and the Gulf of

Mexico, and specifying open boundaries in deep ocean gave the most accurate surge predictions, compared to those obtained from computation on smaller grid domains including only the Gulf of Mexico, or the continental shelf near Florida coast, respectively.

As mentioned in the previous section, storm surge at the coast results from the interaction between meteorological wind forcing and geometric factors. On the other hand, storm surge in the deep water is mainly induced by the pressure deficit and hardly affected by the surface wind stress or the offshore landscape. Therefore, storm surges at the open boundary in deep water are readily estimated by Eqn.(2.4). Furthermore, it is found that storm surges initiated from the surge rise on the deep ocean boundary and forced to propagate toward coastal regions in more natural fashion could avoid the erroneous excitement (Westerink et al., 1991) in coastal water level as well as reduce error potential due to complicated specification across the continentally boundary.

Westerink et al. (1991 and 1992) examined the improvement in the accuracy with respect to the grid refinement for coastal surge prediction. They concluded that, to obtain the relevant accuracy in surge level computation, a high degree of grid refinement was required to resolve complex geometry and rapidly varying bathymetry in shallow water regions while much lower grid resolution was found to be sufficient for the deep water part. For efficient use of computational resources, they further developed a mesh grid with varying resolution that has coarse refinement in deep waters and gets finer toward coastal regions. It was proved that surge response obtained by using the varying-resolution grid could be identical to that obtained by using the uniformly fine grid.

To obtain flexibility in nodal densities of a mesh grid, the shallow water equations are solved by the finite element (FE) method with various algorithms (Navon, 1988; Gray, 1982). With the development of the Wave-Continuity Equation (WCE, Lynch and Gray, 1979) that implements the primitive mass continuity and momentum conservation, spurious node-to-node oscillation commonly found in early FE numerical models was suppressed without artificial damping . Using the operator notation, a WCE (W) is presented (Lynch and Gray, 1979; Aldama et al., 2000; Kolar and Westerink, 2000) as

$$W \equiv \frac{\partial L}{\partial t} + \tau L - \nabla \bullet \mathrm{M}^{\mathrm{C}} = 0 \tag{2.6}$$

where
L represents the primitive form of mass continuity,
M^c represents primitive form of momentum conservation, and
τ is the bottom friction factor.

Kinmark et al.'s (1985) work on refining the previous WCE resulted in the Generalized Wave-Continuity Equation (GWCE). By replacing the bottom friction factor, τ with the weight factor, G associated with the primitive continuity of mass equation, L, the GWCE (W^G) is formulated (Luettich et al., 1991 and Kolar and Westerink, 2000) as

$$W^G \equiv \frac{\partial L}{\partial t} + GL - \nabla \bullet \mathrm{M}^{\mathrm{C}} = 0 \tag{2.7}$$

Here, the G parameter has no physical meaning but is introduced as a means for describing a wide class of equations, including the wave continuity equation itself, for

numerical solutions. By choosing as large value of G as possible that satisfies $G > \tau$ so Eqn. (2.7) has a nontrivial solution, yet the GWCE remains equivalent to the primitive WCE, the spurious oscillation problem can be avoided without artificial damping. Furthermore, by virtue of the flexibility in the value of G, the GWCE can be explicitly solved using time-independent mass matrices for elevation solutions.

The objective of the literature review in this section is to provide an overview of surge model development, to help one understand about the principle physics behind storm surge and to build a fundamental idea of the advantages gained from the advance in modeling schemes. Therefore, lengthy description on the numerical schemes or details that require in-depth understanding about the numerical analysis method is not included here.

2.4 Review of Extreme-Value Statistics for Storm Surge

Since the 1960's, a number of efforts have been made to characterize hurricane hazard in terms of its surge and frequency. However, early methods depended on historical hurricane data recorded in small spatial scale over a short period. Furthermore, the early hurricane record did not contain more intense storms that have occurred since 1960's. Therefore, reliance on such a paucity of weak data resulted in a high degree of uncertainties in the extreme-value analysis from various factors.

For example, in the Design Storm approach developed as a part of the Standard Project Hurricane (SPH, U.S. Department of Commerce, 1959, 1972, and 1979) work, a hurricane's behavior was characterized by only one parameter, typically the storm intensity, and disregarded the variability of other factors. Also surge levels are analyzed

based on a single storm, designed based on environmental conditions seen in the limited historical data. Such an approach ignores possible changes in hurricane conditions in the future.

Since the period of high hurricane activities in the 1960's, many researchers put effort into developing the parametric (Gumbel, 1959) or non-parametric or empirical (Borgman et al., 1992; Scheffner et al., 1996) representations of historical storm surge data, as a means for extreme surge analysis. However, such a reliance on the limited historical data infers the statistics had some potential problems. First, the historical population cannot capture the changes in frequencies and intensities of storms on decadal scales. Second, this approach does not account for the spatial extent over which the hurricane surge acts.

Ho and Myers (1975) developed a statistical approach that utilizes the joint probability function to describe storm surge probability on certain condition. This method, termed as JPM (Joint Probability Method), first specifies various hurricane parameters ($x_1, x_2, ..., x_n$), such as the storm size, intensity, speed, and so forth. With the specified parameters, the CDF (Cumulative Distribution Function) for a hurricane with specified condition $x_1, x_2, ..., x_n$ will generate surge level in excess of a certain surge value, η, is evaluated as

$$F(\eta) = \int ... \int p(x_1, x_2, ..., x_n) \delta[\Psi(x_1, x_2, ..., x_n) - \eta] dx_1 dx_2 ... dx_n \qquad (2.8)$$

where
η is the threshold of the highest surge at a given location,
$p(x_1, x_2, ..., x_n)$ is a joint probability for a event caused by the combination of variables $x_1, x_2, ..., x_n$,
$\delta[..]$ is the Dirac delta function,
$\Psi(x_1, x_2, \ldots, x_n)$ is a numerical model for surge estimation based on the variables $[x_1, x_2, ..., x_n]$
, and n is the total number of hurricane parameters.

In its original form, the JPM does not acknowledge that the numerical model computation may not be 100% accurate or/and that the joint probabilities estimated from a small sample size may not exactly represent the parent group. Furthermore, assuming the structure of storms change very slowly during its approach to the coast, this approach regards the hurricane condition off the coast as the same as that at landfall, which the recent data shows be not true (Resio et al., 2009). Moreover, the JPM approach produces the storm surge information based on the joint probabilities among a large variety of hurricane variables. Therefore, for accumulating sufficient surge data, the JMP approach requires heavy computational work.

Resio et al. (2009) suggested that improved statistical surge analysis should have a means to justify the errors. These errors may be produced by the inexact assumption applied for the hurricane modeling and computation, uncertainties in characterizing the joint probabilities from limited data, uncertainties in unknown events in the future, and uncertainties in possible changes in present conditions. Furthermore, careful consideration on the effect of hurricane evolution required as hurricanes approach the coast, and to the variability in the structure of the hurricane wind field.

CHAPTER III

STUDY AREA: TWENTY COASTAL BRIDGES ALONG THE TEXAS COAST

First, the examination of satellite images of the Texas coast was conducted to determine the study area where high inundation is suspected. After consideration of the bridges' locations with respect to the regional geography, and their importance to the nearby neighborhood, twenty bridges along the Texas coast were selected for examination for their vulnerability to hurricane flooding (Fig. 3). The geographical features near a subset of these bridges are shown in Fig. 4 through Fig. 11.

As shown through figures, most of the bridges located on the open coast are exposed to a direct strike from incident surges and waves developed in the Gulf of Mexico and on the continental shelf, while some in the adjacent basins are subjected to inundation due to flooding invasion through tidal inlets or over the barrier islands. Locations of the bridges are summarized in Table 1, along with the numbers of corresponding output stations specified on for the hurricane simulations.

In the middle of thesis development, Hurricane Ike (2008) emerged into the Gulf of Mexico and made landfall near Galveston. Due to this hurricane, several coastal bridges near Galveston Bay were damaged. Our target bridges include two of these severely damaged bridges (Fig. 12): Rollover Pass Bridge (Fig. 5 and on the top of Fig. 13), located on Bolivar Peninsula and Pelican Island Bridge (Fig. 6 and on the bottom of Fig. 13) located in Galveston. Malfunction of these damaged bridges cut off the public transportation system, delayed restoration after the disaster (Jones 2009), and cost about $7 million to repair (Rappleye 2008).

The estimation of storm surge levels near these selected bridges can be made through numerical model study and use of SRF. Surge development is determined by hurricane meteorology, geographic properties of the region, such as bay geometry, variation in bathymetry, and shoreline shape. Since our target bridges are placed over a wide range of the Texas coast, an enormous number of storm surge simulations would be required to assess flooding probability with a traditional JPM approach. However, by adopting the SRF approach introduced by Resio et al. (2009; see CHAPTER IV), the number of simulations required for characterizing the site-dependent surge response behavior may be dramatically decreased.

In the following chapters, details of the SRF concept, along with the relevant theories and overview of the conventional surge analysis method, will be reviewed.

Fig. 3 Locations of twenty target bridges along Texas coast (red dots). (from Google Satellite Images, 2009a)

Fig. 4 Bridges (the red circles) near the eastern boundary of the Texas coast. Jetty Road (right) and Martin Luther King Jr. Drive (Hwy 82, left) are located near the eastern boundary of Texas. (from Google Satellite Image, 2009b)

Fig. 5 A bridge (the red circle) at Rollover Pass in Galveston. (from Google Satellite Image, 2009)

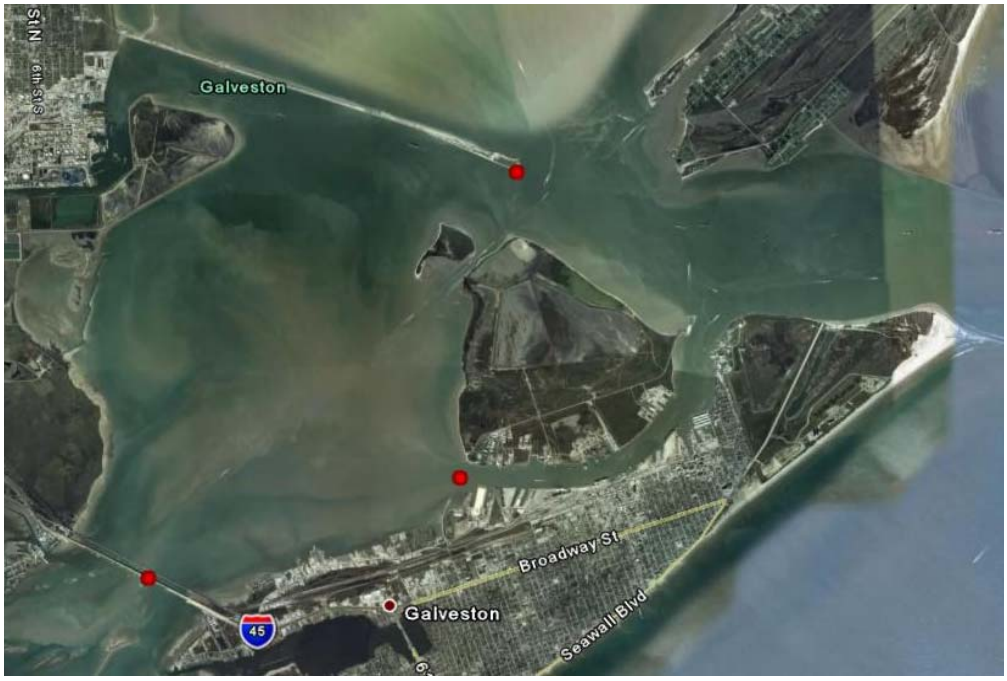

Fig. 6 Bridges (the red circles) near the entrance of Galveston Bay. Bridges are located on the Texas City Dike Road (top, right), Pelican Island Bridge (middle), Galveston Causeway (bottom, left) near the entrance of the Galveston Bay, respectively. (from Google Satellite Image, 2009d)

Fig. 7 Bridges (the red circles) of FM 2004 Road (top), and San Luis Pass (bottom) in Galveston. (from Google Satellite Image, 2009e)

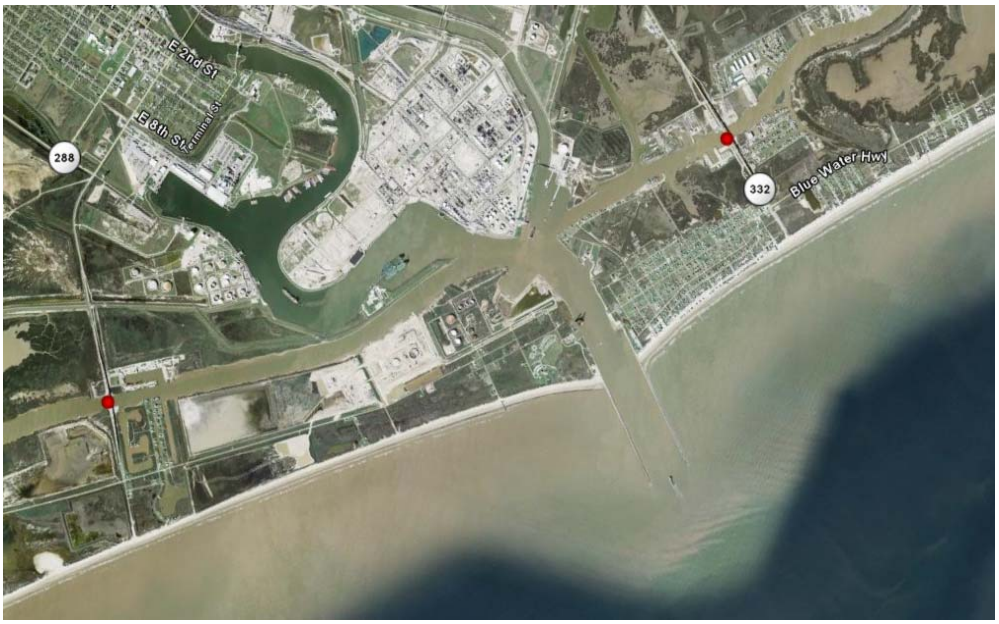

Fig. 8 Bridges (the red circles) on FM1495 Road (left) and Hwy 332 (right) near Freeport. (from Google Satellite Image, 2009f)

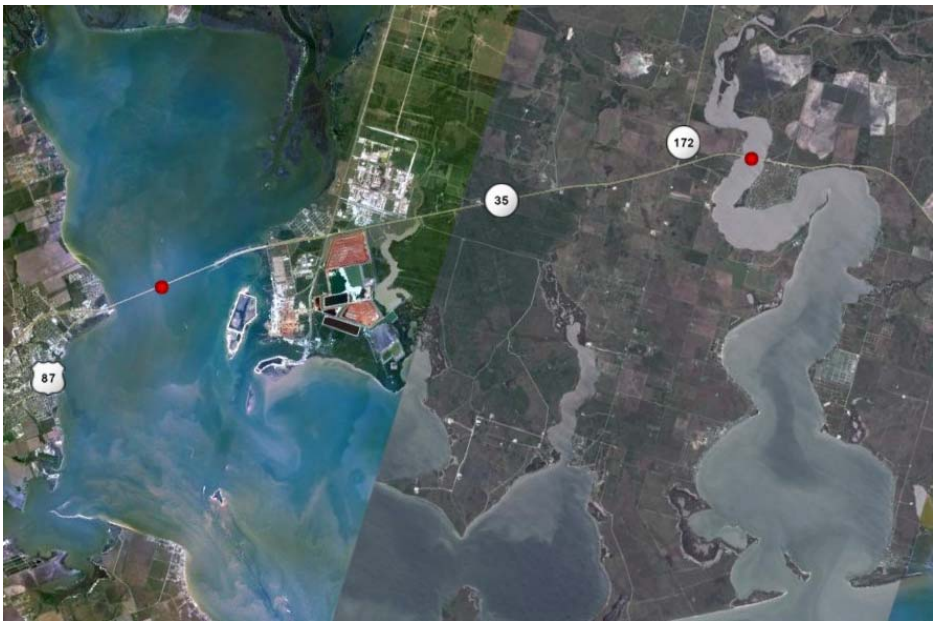

Fig. 9 Bridges (the red circles) along Highway 35 in Matagorda Bay. (from Google Satellite Image, 2009g)

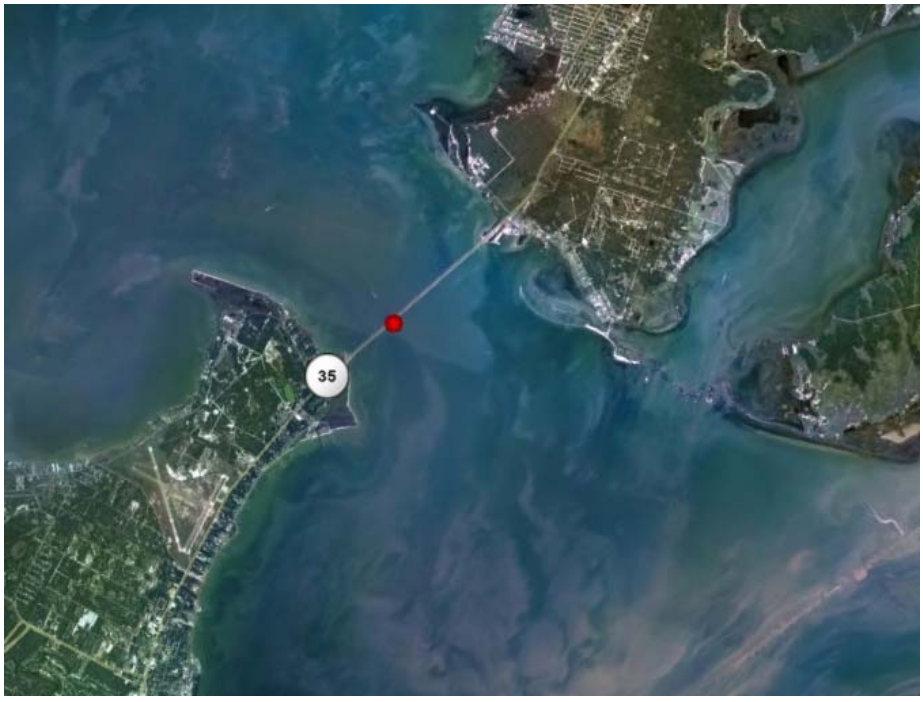

Fig. 10 A Bridge (the red circles) on Lyndon B. Johnson Causeway in Aransas. (from Google Satellite Image, 2009h)

Fig. 11 Bridges in Corpus Christi. A bridge (the red circle, clockwise, from the left)) on State hwy Park Road 53, two bridges on State Hwy Park Road 22, one on the Padre Island Drive, a bridge over the industrial canal, and two bridges on Cemetery Road, Nueces Bay Causeway, respectively. (from Google Satellite Image, 2009i)

Table 1. Locations of the selected coastal bridges

Bridge No.	Stn. No.	Description	Lon.	Lat	Location
1	45	State Hwy Park Road 22_No.1	-97.214	27.619	Corpus Christi
2	49	State Hwy Park Road 22_No.2	-97.240	27.635	
3	48	Kennedy Causeway	-97.261	27.658	
4	51	Padre Island Bridge	-97.312	27.680	
5	53	Nueces Bay Causeway 1	-97.395	27.813	
6	55	Nueces Bay Causeway 2	-97.370	27.844	
7	59	Cemetery Road	-97.104	27.884	
8	65	Johnson Causeway	-97.020	28.120	
9	84	Port Lavaca	-96.598	28.650	Matagorda
10	88	Weedhaven	-96.432	28.732	
11	116	FM1495 Road	-95.341	28.922	Galveston
12	117	Hwy 332	-95.293	28.956	
13	127	San Luis Pass	-95.122	29.082	
14	130	FM 2004 Road	-95.207	29.213	
15	141	Galveston Causeway	-94.885	29.295	
16	142	Pelican Island Bridge	-94.824	29.311	
17	147	Texas City Dike Road	-94.810	29.363	
18	157	Rollover Pass	-94.500	29.508	
19	181	Martin Luther King Jr. Drive (Hwy 82)	-93.895	29.766	
20	182	Jetty Road	-93.853	29.696	

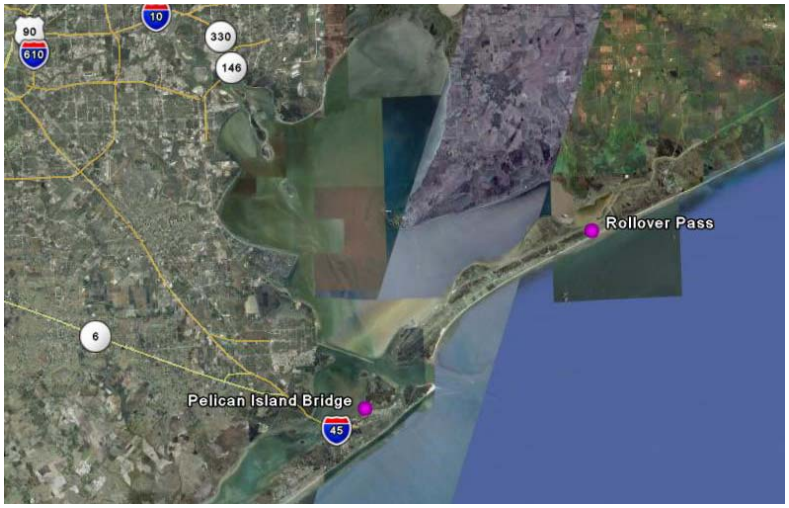

Fig. 12 Location (marked by maroon dots) of two damaged bridges in Galveston during Hurricane Ike (from Google Satellite Image, 2009j)

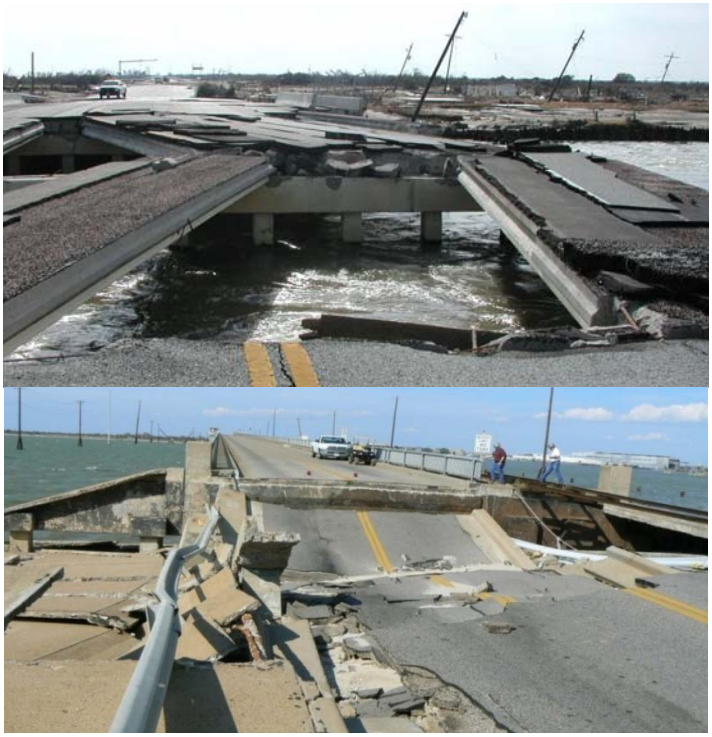

Fig. 13 Bridge damage during Hurricane Ike. Two bridges damaged during Hurricane Ike. Rollover Pass located between the communities of Gilchrist and Caplen (top). Pelican Island Bridge along the 51st Street over the Galveston Ship Channel (photos courtesy of Dr. Jun Jin (2008), Texas A&M University)

CHAPTER IV

METHODOLOGY

In order to measure the uplift force and impact of debris on the selected coastal bridges during hurricanes, prediction of flood level derived hurricane meteorology is required. There is only scarce historical hurricane data available at theses bridges to estimate the storm surge probability from the historical record alone. Therefore, storm surge data at each bridge location had to be accumulated through numerical simulation. In an effort to avoid heavy computational burden imposed by the great amount of hurricane simulations typically required to quantify surges over a wide range of storm conditions along the entire Texas coast, optimal sampling from a synthetic hurricane wind field database was carried out. Following the modified JPM approach suggested by Resio et al. (2009), hurricane parameters which have the most dominant effects on the storm surge response were first selected. Furthermore, subsets for storm surge simulations were determined based on careful combination of the selected parameters. Then, storm surge model study for evaluating extreme surge levels near twenty target bridges is conducted. Finally, the simulated surge data were analyzed to develop parameterized surge response functions, in order to evaluate surges on wide range of hurricane meteorological conditions near the target bridges.

4.1 Surge Response Function Approach for Joint Probability Method with Optimal Sampling

To develop the improved methodology for surge hazard analysis, Resio et al. (2009) introduced a modified joint probability method implementing the SRFs. In this method, the number of variables used for joint probability in Eqn. (2.8) is limited to include only those hurricane parameters that have the most dominant effects on surge response, based on physical reasoning. This process is called optimal sampling and the original JPM is now revised to be Joint Probability Method with Optimal Sampling (JPM-OS). Furthermore, the JPM-OS specifies the error term, ε, to incorporate the storm surges with uncertainties from various sources. That is, the effect of the variation in surges due to other factors than those classified as dominant factors is regarded as negligible and swept into the error term.

The strength of the surge response approach is in that it characterizes the storm surge response of the surface water by the physical correlations between surges and the meteorological hurricane parameters. As discussed earlier, a large portion of storm surge is generated by hurricane wind stress and pressure deficit forcing. Consequently, it would physically make sense that the dominant parameters in JPM should correspond to those parameters utilized to describe the wind field. The hurricane wind field can be parameterized with respect to the location of eye, storm size, intensity, forward speed and angle, and pressure profile peakedness. Therefore, the modified joint probability distribution with reduced dimensions, where the error term is separated from the probability distribution, is integrated into the CDF

$$F(\eta) = \int ... \int p(c_p, R_p, v_f, \theta_l, x_o, B)\, p(\varepsilon \mid \eta) H[\eta - \Psi(\overrightarrow{X}) + \varepsilon] dx_1 dx_2 ... dx_n d\varepsilon \qquad (4.1)$$

$$\Psi(\overrightarrow{X}) = \Psi(c_p, R_p, v_f, \theta_l, x_{eye}, B) \qquad (4.2)$$

where

R_p is the storm pressure radius,

c_p is the storm central pressure,

B is the pressure field structure peakedness (Holland B,1980),

x_{eye} is the location of storm eye,

v_f is the storm forward speed,

θ_l is the storm approach angle, and

$\Psi(\overrightarrow{X})$ is a numerical model or system.

Here, the error term ε also provides a means to include other effects on the water levels such as tides and waves.

The storm surge probability expressed as Eqn. (2.10) is even more reduced by using mean value of the profile shape factor, Holland B ($\overline{B}$, 1980). By considering the Holland B as constant (Resio et al., 2009), the dimension of storm surge joint probability is reduced to

$$p(\overrightarrow{X}) = p(c_p, R_p, v_f, \theta_l, x_{eye}) \qquad (4.3)$$

Finally, the continuous hurricane probability is obtained by,

$$F(\eta) = \int ... \int p(c_p, R_p, v_f, \theta_l, x_{eye})\, p(\varepsilon \mid \eta) H[\eta - \Psi(\overrightarrow{X}) + \varepsilon] dx_1 dx_2 ... dx_n d\varepsilon \qquad (4.4)$$

Eqn. (2.12) shows that hurricane distribution of surge level η can be represented by a continuous function of primary hurricane parameters.

Now, if we make our focus on the maximum surge level $\eta_{\max}$ at an arbitrary location (x, y) against random sets of hurricane condition, the Eqn. (2.12) may re-write as

$$\eta_{\max}(x, y) = \phi(c_p, R_p, v_f, \theta_l, x_{eye}) \tag{4.5}$$

where ϕ represents the surge response function characterizing the correlations between surges and the dominant hurricane parameters.

4.2 Surge Response Function Methodology

Resio et al. (2009) performed intensive numerical studies to examine the sensitivity of storm surge level to the dominant hurricane parameters. They concluded that the surge behavior when specified mainly by hurricane intensity ($\Delta P = P_f - c_p$), where P_f is a far-field pressure, and storm size (R_p). On the other hand, surge variations with respect to storm approach angle (θ_l) or speed (v_f) are seen to be somewhat less important (Irish et al., 2009). That is, for two close locations, a fixed value of approach angle (θ_l) and speed (v_f) can be used as an initial evaluation of surge response. Therefore, at a spatial point $(x, y)_n$ where the storm approach angle with respect to shoreline orientation (θ_l) and speed (v_f) may be regarded as a fixed value of k and m, respectively, the maximum storm surge ζ can be described in terms of hurricane meteorology; ΔP , R_p , (x, y), and a location of eye at landfall (x_o, y_o) as (Irish et al., 2009);

$$\zeta(x, y) = \phi_{km}([x, y], \Delta p, R_p, [x_o, y_o]) \tag{4.6}$$

The SRF approach, required for efficient use of the JPM –OS, enables the reliable estimation for the extreme surge flood levels based on a reasonably selected sample. Also, it provides a means to account for the errors due to uncertainties in assumptions and simplifications made during the surge development process. Eqn. (4.6) shows that, at a given location, the maximum storm surge surface (ζ) can be described by a continuous function of hurricane parameters and site-dependent geographic properties. Irish et al. (2009) has developed dimensionless parameters based on physical scaling laws that relate the hurricane meteorology and location to the maximum surge levels. Products of the scaling process were interpolated to construct a Surge Response Function (SRF), demonstrating the continuous surge response behavior on various hurricane conditions with respect to the alongshore extent.

Furthermore, Irish et al. (2009) provided a standard for optimal sampling for surge response analysis in order to minimize the computational requirement for hurricane model simulation while maximizing the use of existing discrete sets of surge data.

In the following sections, we will present the physical scaling laws of Irish et al. (2009) used to derive dimensionless storm surge parameters. Then, we discuss how, in this thesis, this method was improved and applied for extreme surge prediction at vicinity of the Texas coast.

4.2.1 Physical Scaling Laws for Surge Response Function

Irish et al. (2009) performed 75 numerical storm surge simulations along a stretch of the Texas coast, near Matagorda Bay. This investigation focused on storms

propagating toward the coast of Matagorda Bay with an approach angle of less than 17°, with respect to shore-normal, along four parallel tracks spaced 30km apart from each other (Fig. 14). The 75 synthetic hurricanes varied in intensity (c_p) from 900mb to 960mb and in size (R_p) from 11km to 65km. For each track, at least five different properties were specified for storm intensity in order to create the synthetic hurricane wind field, in combination with at least five storm size specifications. The changes in coastline and nearshore bathymetry within the study area are slow and smooth, and the four stations specified for surge output recording are close enough to each other. Forward speed and Holland B of each hurricane were specified as 5.7m/s and between 1.27 and 1.00, respectively, which are typical values for hurricanes in Gulf of Mexico.

From the simulated surge results, Irish et al. (2009) identified a linear correlation between storm size and the alongshore distance between the eye at landfall and the location of peak surge. The relationship was described by using a parameter λ as

$$x_{\zeta_{peak}} - x_o \cong \lambda R_p \tag{4.7}$$

where
x_{peak} is a alongshore distance to the location of the peak surge
x_o is a alongshore distance to the location of eye at landfall, and
and R_p is the hurricane pressure radius.

Note that spatial extent was measured along the shoreline at the open coast, for purpose of evaluating storm surge responses with respect to the variation in relative distance from the eye of storm to the arbitrary point.

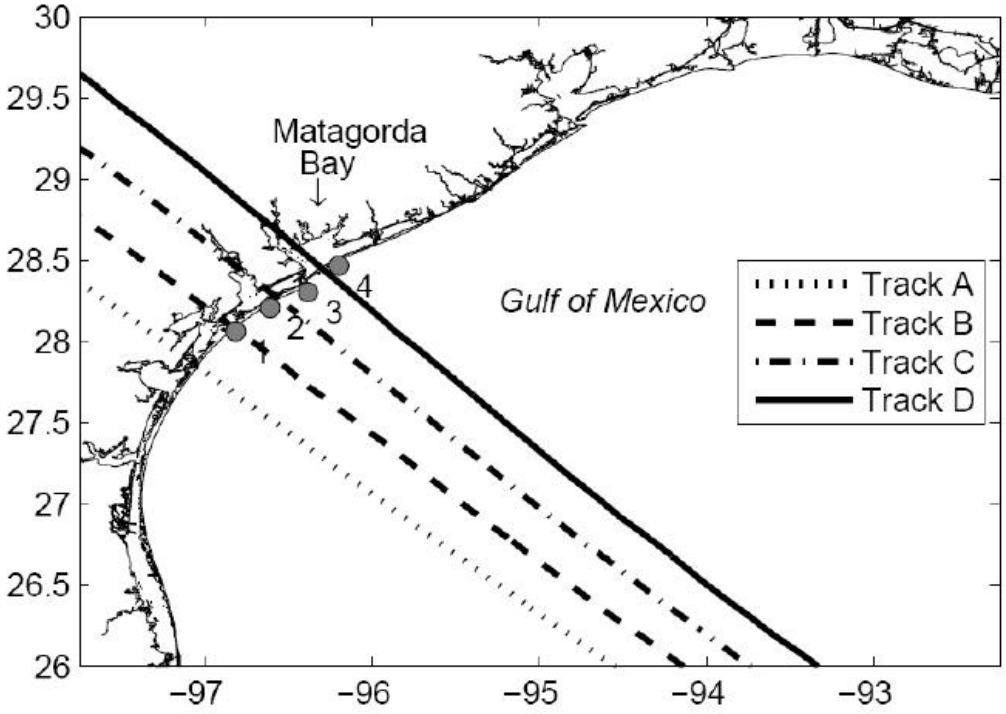

Fig. 14 Hurricane tracks and stations for SRF development (from Irish et al., 2009). The circles mark sample output locations.

For extreme-value statistics, our interest was in higher surge events. A dimensionless alongshore dimension (*x*') representing the distance from landfall of a hurricane to the point of interest (i.e. a location of surge monitoring stations) was defined as

$$x' = \frac{x - x_o}{R_p} - \lambda \tag{4.8}$$

The authors also defined a dimensionless surge parameter (ζ') by normalizing simulated surge levels by hurricane intensity.

$$\zeta' = \frac{\gamma\zeta}{\Delta p} + m_x \Delta p \tag{4.9}$$

The first term in Eqn. (4.9) accounts for the storm surge as a response to the momentum transfer due to the surface wind stress. The second term accounts for additional wind-drag effect. The coefficient m_x is a site-dependent coefficient and determined by linear regression.

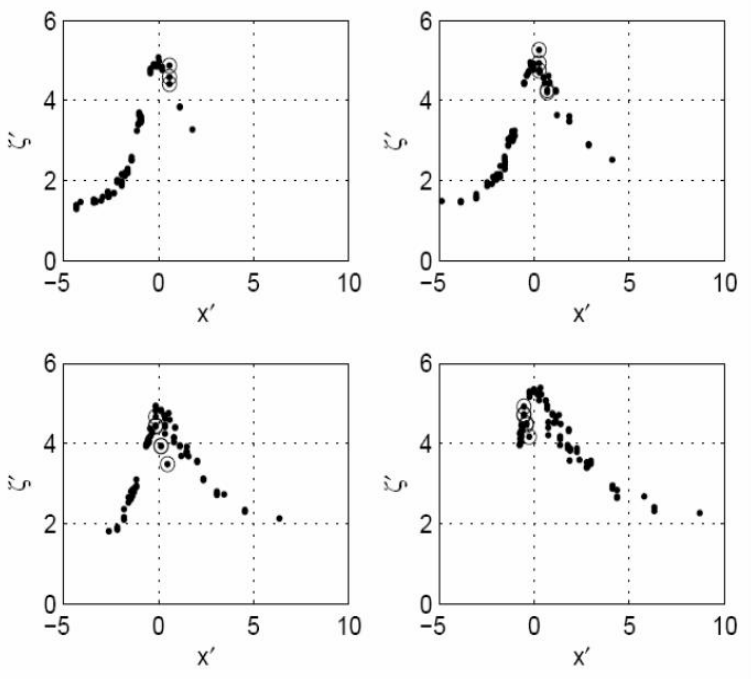

Fig. 15 Preliminary dimensionless SRFs (from Irish et al., 2009). SRFs were developed by using all simulated storms on all four tracks for Locations 1 (top left), 2 (top right), 3 (bottom left), and 4 (bottom right). Circled storms are those with *Rp* < 25 km and -λ< *x'* < λ

Fig. 15 shows plots of the two dimensionless parameters defined by Eqn. (4.8) and (4.9). Overall data distribution follows a single distribution function. However, there were a few prominent scatters near the peak of the distribution. In analyzing those storms, which did not follow the trend, it was determined that these storms where

relatively small storms making landfall close to the point of interest. This class of relatively small storms was classified as storms with $R_p < R_{thres}$ and $-\lambda < x' < \lambda$, and the threshold size was estimated by inspection to be R_{thres}=25km, in the vicinity of Matagorda Bay.

To collapse this class of storms into the single distribution function obtained before, the dimensionless alongshore parameter (x') was revised and redefined:

$$X'_2 = X' - F(1-R')H(1-R') \tag{4.10}$$

where *R'* is the dimensionless hurricane size defined as $R' = R_p/R_{thres}$, $H(1\text{-}R')$ is the Heaviside function defined as

$$H(1-R') = \begin{cases} 0 & (R' \geq 0) \\ 1 & (otherwise) \end{cases} \tag{4.11}$$

$F(1\text{-}R')$ is a ramp function defined as:

$$F(1-R') = \begin{cases} a_1(1-R') + b_1 & (\lambda \leq x' \leq 0) \\ a_2(1-R') + b_2 & (0 \leq x' \leq \lambda) \\ 0 & (\lambda \leq |x'|) \end{cases} \tag{4.12}$$

The coefficients a1, a2, b2, and b2 of the ramp function were evaluated by linear regression between the quantity (1-R') and the difference between the value of x' and x2' corresponding to the ζ' from existing surge distributions. Fig. 16 shows the plots of revised dimensionless parameters. The figure shows that the data distribution follows a single trend after the secondary effects from small storms are tuned.

The relationship between x'2 and ζ' were formulated through curve-fitting using a three-term Gaussian distribution function as

$$\Phi(x') = a_1 e^{-\left(\frac{x'-b_1}{c_1}\right)^2} + a_2 e^{-\left(\frac{x'-b_2}{c_2}\right)^2} + a_3 e^{-\left(\frac{x'-b_3}{c_3}\right)^2} \tag{4.13}$$

By the least squares regression method, curve-fitting coefficients *a1*, *b1*, *c1*, *a2*, *b2*, *c2*, *a3*, *b3*, and *c3* were determined (Fig. 16). Irish et al. (2009) reported R-squared values of curve-fits at four stations were evaluated between 0.97 and 0.99. The comparison of the predicted surges from the SRF (ζ_Φ) to the numerically simulated surges (ζ_{sim}) showed the root-mean-square (RMS) errors varied from 13 cm to 24 cm (Fig. 17), and is on the order of the numerical simulation accuracy.

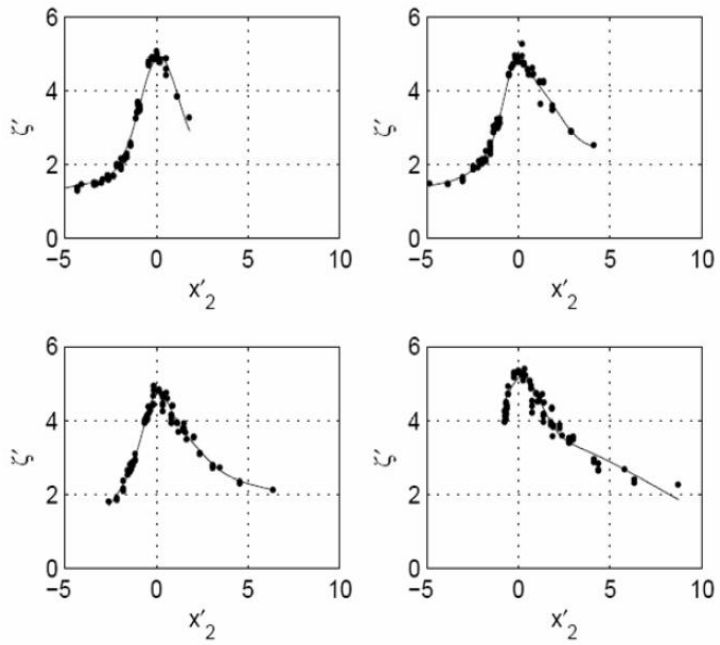

Fig. 16 Dimensionless SRFs using the modified dimensionless alongshore parameter (from Irish et al., 2009). SRFs were developed by using all simulated storms on all four tracks for Locations 1 (top left), 2 (top right), 3 (bottom left), and 4 (bottom right). Solid line shows 3-term Gaussian fit to data.

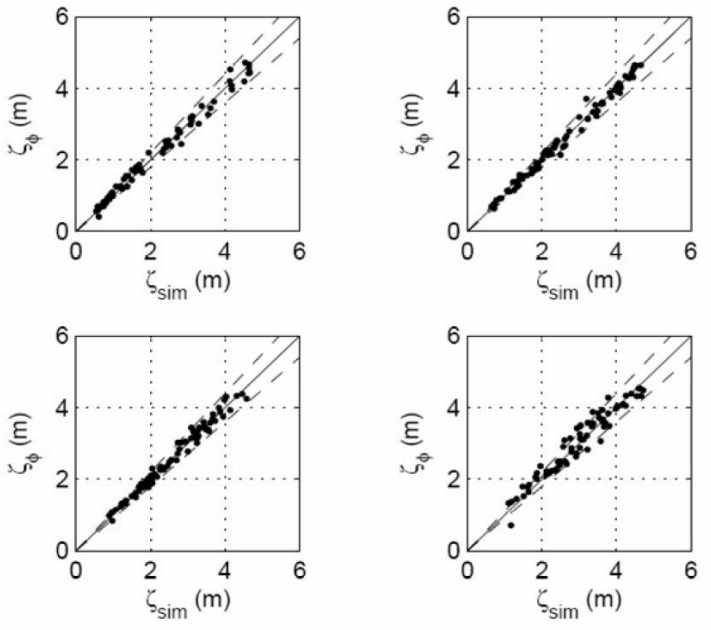

Fig. 17 SRF Prediction versus numerically simulated surges (from Irish et al.,2009). Predicted surge using curve-fitted SRF, based on all four tracks, versus numerically simulated surge at Locations 1 (top left), 2 (top right), 3 (bottom left), and 4 (bottom right). Solid line indicates an exact match while dashed lines indicate ±10% about an exact match.

4.2.2 Surge Response Function from Limited Data

Irish et al. (2009) further examined the use and accuracy of dimensionless SRFs from limited data sets. First, in order to examine the maximum track spacing for accurate SRF development, 75 hurricanes were sorted into three groups; hurricane tracks separated (1) 30km (0.25°), (2) 60km (0.50°), and (3) 90km (0.75°). As a result, the SRF developed from hurricanes in the third group was found to be as accurate as that generated from the first group, as long as data exists on both sides of $x_2^{'}$=0, and in the vicinity of the peak in the SRF. Therefore, up to 90km intervals between the storm tracks

were found to be sufficient for defining the hurricane sample to be used to develop accurate SRFs. Also, the authors showed that storm surges from only two discrete storm intensities, C_p =900mb and 960mb were sufficient to generate the SRF with the same order of accuracy, compared to what was generated from all 75 numerical simulations. Analysis of those limited data sets proved that the use of the SRF approach can effectively reduce the numerical simulation requirement by at least 75% without loss in surge estimation accuracy.

4.3 Improvement for General Use of Surge Response Functions

It should be emphasized that in their original work, Irish et al. (2009) have focused on the open coast near Matagorda Bay. In this region, the relative impact of alongshore change in topographic (i.e. bottom slope) and geographic (i.e. shoreline orientation) conditions from location to location was insignificant. Thus, the assumption of slowly varying shoreline conditions was applied. Additionally, the storms for all storm surge simulations were forced with one forward speed and approach angle. Thus the SRF work of Irish et al. (2009) excludes the effects of different forward speeds, approaching angles, and excludes the effect of variation in regional bathymetry.

On the other hand, the coastal bridges selected for this thesis are widely distributed throughout the Texas coast. Therefore, the spatial scope for this study is expanded to include three main Texas bays: Galveston, Corpus Christi, and Matagorda. Consequently, some assumption and simplification applied to the previous work was revaluated. In particular, application of SRFs to comprise a wider range of the Texas coast should take the effects of varying bottom slope, or continental shelf width into

account. The storm surge level at the coast is affected by bottom slope of the site as expressed in Eqn. (2.5). It was found that more than 75% of surge is generated as the hurricane moves over the continental shelf in depths shallower than 30 m (Irish and Resio, 2009). Fig. 18 is the Texas coast map displaying the coastline shape and the continental shelf expansion from the coast to the 30m water depth contour; this detour will be termed L30 from this point. The figure clearly shows that L30 gets rapidly wider, while the change in shoreline orientation remains insignificant. Therefore, the change in L30 in relation to surge generation is investigated for this study. Thus, we investigate the need to redefine the site-dependent coefficients or introduce a new parameter that accounts for the effect of changes in such geographical conditions.

In the derivation of dimensionless surge (ζ'), Irish et al. (2009) did not explicitly include the effect of storm size in the physical scaling law in Eqn. (4.9). However, a number of recent studies for hurricane impact analysis have proved that both the size and the intensity of storms play important role in surge generation (Irish et al., 2008; Powell and Reinhold, 2007; Resio and Westerink, 2008). Through analysis of both the historical records and numerical computation, it was further evidenced that a storm of moderate intensity with a large size could generate more devastating storm surges (Katrina, 2005; Ike, 2008) than could another storm of stronger intensity but with a smaller size (Irish et al., 2008). Recognizing the contribution of the storm size to storm surge generation, the work to establish the physical law relating the size to the storm surge levels is in process. Meanwhile, in this thesis, the additional effects due to differences in the size of

simulated storms were resolved through the additional wind drag effects (m_x) in the original dimensionless surge (ζ', Irish et al. 2009).

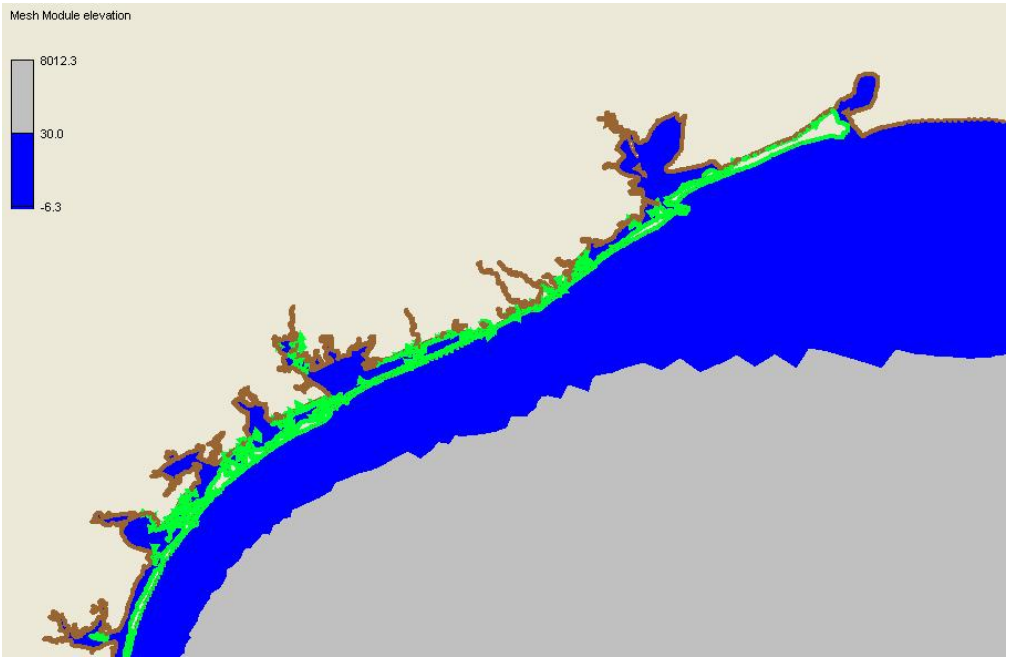

Fig. 18 Texas coastal map of the study area. The area shaded in blue represents the varying continental shelf width (L_{30}) along the Texas coastal line

CHAPTER V

NUMERICAL SIMULATION STRATEGY

To develop sufficient surge data to define and refine SRFs at the selected coastal bridges, numerical hurricane simulations were conducted to compute storm surge levels in the region of interest. In this section, a detailed description is presented on the numerical hurricane simulations is presented. The following presents the numerical storm surge model, ADCIRC, and its setup, hurricane selection, and specification of elevation stations on the open coast.

5 .1 ADCIRC Hydrodynamic Model

For accurate and detailed surge analysis, a storm surge model has to incorporate the key features discussed in this section including:

- A large scale grid domain specifying the open boundary in deep water
- The sufficient grid refinement on the coastal regions including the adjacent basins, and
- The flexibility in node density.

In this study, storm surge elevation was simulated using the advanced hydrodynamic model, ADCIRC-2DDI (Luettich et al., 1991; Westerink et al., 1994). ADCIRC is a surface water circulation model coded using a finite element scheme in space and using a finite different method in time to solve the GWCE, discussed previously in section 2.3.

ADCIRC can be forced by specifying free surface elevations (due to tidal potential or barometric pressures deficit), normal flow, surface stress (due to hurricane wind or wave radiation), and landscape features such as barriers, bridge piers, and so forth. These boundary conditions can be specified on the nodes along the circumference of and/or within the grid domain.

The ADCIRC model provides several options that improve its computational performance. These include the selection of operational mode; the external mode (ADCIRC-2DDI) or internal mode (ADCIRC-3DL), and parallel (MPI-run) or serial processing. In internal mode, ADCIRC computes the vector form of surface water velocities by solving the three-dimensional wave equation with the primitive conservation of momentum. In external mode, ADCIRC computes the scalar of surface water elevations by solving the depth-integrated, two dimensional wave equations with the primitive conservation of mass. ADCIRC execution in external mode saves both CPU time and data storage, requiring on the order of one third that required for the three-dimensional computation. Westerink et al. (2008) showed ADCIRC with this configuration to perform well for surge simulations. Typical computation error for surge simulation is estimated at 20 to 30 cm.

ADCIRC is capable of running on multiple processors in parallel by decomposing the mesh grid and related input files into multiple numbers of smaller pieces, assigning each piece of work to an independent CPU, and then reassembling the output from each CPU back together. In this way, it saves real time taken to complete the total simulation as well as eases the computational burden laid on a single CPU.

ADCIRC is currently utilized to solve the free surface circulation and sediment transport problem by various professional research groups in national institutions including the U.S. Army Corps of Engineers, Federal Emergency Management Agency (FEMA), National Laboratory for Civil Engineering (LNEC), National Oceanic and Atmospheric Administration (NOAA), and U.S. Naval Research Laboratory (NRL).

5.1.1 Computational Domain

As a model domain, the east coast computation domain of Westerink et al. (2008) was used. This grid include the Western North Atlantic Ocean, the Caribbean Sea, and the Gulf of Mexico is used (Fig. 19). The east coast domain specifies open boundaries along the 60°W meridian, and the grid refinement widely varies from about 0.400° in the deep ocean to 0.005° nearshore and in inland bays (Weterink et al., 1992 and 1994). Especially, it highly resolves the regional bathymetry near the Texas coast and adjacent bays and waterways. Detailed grid information lists in Table 2.

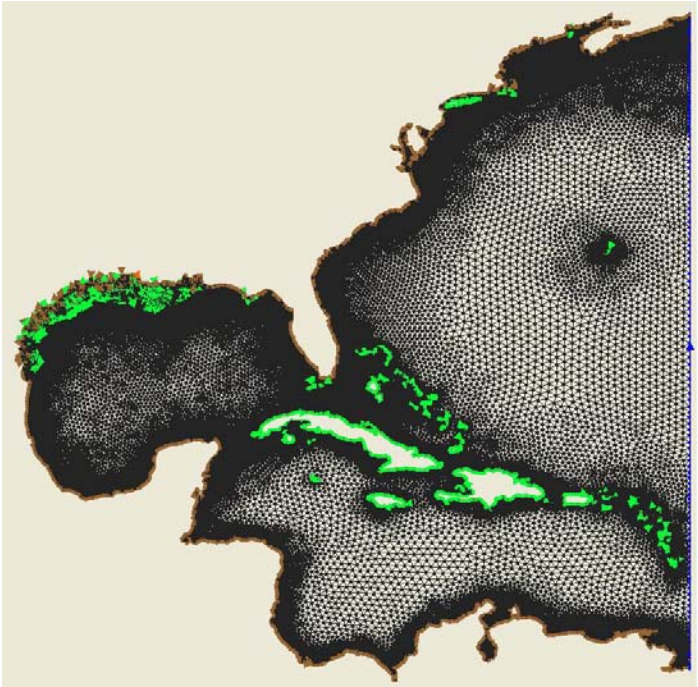

Fig. 19 East coast ADCIRC domain grid.

Table 2. East coast domain triangular mesh information

Area [km^2]	Maximum Bathymetry [m]	Minimum Bathymetry [m]	Number of Nodes	Number of Elements	Grid size (Approximation, degree)		Grid size (Approximation, meter)	
					Maximum	Minimum	Maximum	Minimum
8.3522×10^6	7,858.09	(-)71.67	1,344,247.00	2,628,785.00	0.400	0.005	46,000	100

5.2 Hurricane Surface Wind Field Modeling

Besides the capability of the storm surge model itself, the accuracy of the surge prediction heavily depends on the accuracy of the specified hurricane forcing. For hurricane simulations, ADCIRC takes hurricane wind and boundary field files containing the information on surface wind and pressure at each time step as input for forcing. Several input wind field sources are available, including reanalyzed historical wind fields (i.e. HWINDS, Powell and Reinhold, 2007). In this thesis, however, we

emphasize parameterization of the surge response, so a parametric wind field model is used. Thus, to develop hurricane wind fields, the Planetary Boundary Layer (PBL) model of Thompson and Cardone (1996) is utilized. This PBL model is derived from the vertically averaged, horizontal equation of motion with respect to a moving cartesian coordinate system with its origin at the center of the eye (Chow, 1971; Cardone et al., 1992). The vertically integrated momentum flux is related to the surface stress, and the wind and pressure fields are represented with respect to hurricane parameters including central pressure (c_p), storm size (R_p), storm forward speed (v_f), and peakedness (B, Holland, 1980). During model development, it was assumed that the vortex flux within the PBL is horizontally homogeneous, steady state, and that the structure of a hurricane wind field changes slowly (over periods longer than one hour). Therefore, properties of those hurricane parameters are specified at one hour interval, and based on this information the PBL model computes the wind velocities and pressure at the nested grid points at specified time steps. For this study, in order to adequately resolve the temporal surge response as the hurricane moves over the continental shelf and the landmass, wind speed and pressure were set to be read every fifteen minutes in a format compatible to ADCIRC file specification. The PBL model uses a moving coordinate system so the origin of the nested grid always coincides at the center of the hurricane. The nested domain is constructed by overlapping seven regular grids, each with progressively coarser grid spacing (1.25km, 2.5km, 5km, 10km, 20km, 40km, and 80km) from the origin of the coordinate system. Therefore, grid refinement can be efficiently adjusted so the complete grid has high resolution near the center of the eye and low resolution

outside the radius where spatial variation in hurricane wind diminishes. The PBL model converts wind (x and y direction, respectively) and pressure information into a format compatible to ADCIRC specification so the PBL output is directly used as wind and pressure field input forcing for ADCRIC storm surge simulation. Given the hurricane forcing, ADCIRC calculates surface wind stress following Garratt's (1977) relationship as

$$\frac{\tau_x}{\rho_o} = C_{D,x}\frac{\rho_a}{\rho_o}|W_{10}|W_{10,x} \tag{5.1}$$

$$\frac{\tau_y}{\rho_o} = C_{D,x}\frac{\rho_a}{\rho_o}|W_{10}|W_{10,y} \tag{5.2}$$

where

τ_x, τ_y is wind stress in the x and y direction, respectively,

$\frac{\rho_a}{\rho_o}$ is ratio of air density to average density ofseawater,

$W_{10,x}, W_{10,y}$ is x and y component of wind velocity vector at a 10m height in units of m/s,

$|W_{10}|$ is wind speed at a 10m height in units of m/s, and

C_D is Garratt's (1977) frictional drag coefficient defined as

$$C_{D,x} = (0.75 + 0.067W_{10,x}) \times 10^{-3}$$
$$C_{D,y} = (0.75 + 0.067W_{10,y}) \times 10^{-3}$$

The PBL specifies the hurricane pressure field, P_c following the exponential law (Holland B, 1980) as

$$P_c = P_{eye} + \Delta P e^{-(R_p/r)^B} \tag{5.3}$$

where

P_{eye} is pressure at the eye of the storm,

ΔP is pressure deficit,

r is the distance from the eye of the storm, and

R_p is a pressure scale radius used in PBL model.

Including Holland B for the parametric expression of observed hurricane intensity also improves the accuracy in the maximum wind speed estimation for the hurricane, $U_{\max}$ as

$$U_{\max} = \left(\frac{B}{\rho_a e} \right)^{1/2} (p_n - p_c)^{1/2} \tag{5.4}$$

where e is the base of the natural logarithms. Consequently, the storm surge levels, which would be related to the square of the wind speeds (Irish et al, 2008), were also estimated by linear proportion to the Holland B.

5.3 Hurricane Selection Based on Optimal Sampling

For this study, the sensitivities of surge response to the variation in both forward speed and approach angle were assumed insignificant. Therefore, the storms propagating with 5.7m/s forward speed and less than 17° of angle with respect to shoreline orientation, a typical forward speed and angle of historical hurricanes in Gulf of Mexico (Irish et al., 2009), were only considered. Holland B was held constant at 1.27 until the hurricane is over 50km from landfall; at this point, the hurricane's Holland B was to decrease slowly to 0.9.

As demonstrated previously, the SRF redefines a continuous surge response surface, with respect to relative alongshore distance from the location of the hurricane

eye to the position of interest. In order to measure the alongshore distance, and to investigate the surge responses to varying continental shelf slope, additional 215 elevation stations were specified along the ocean coastline. Accepting the concept of an idealized shoreline, that the surge response at 10m-depth nearshore can represent the overall surge response behavior along the adjacent continental shelf (Irish et al, 2009), the stations were specified along the 10m-depth contour throughout the Texas open coast (Fig. 20).

In addition to the 4 tracks investigated through the preceding work of Irish et al. (2009), a total of 18 storm tracks, 30km apart from each other, were specified to compromise the entire study area (Fig. 20). Specifically, the synthetic storms along eight parallel tracks were selected for surge investigation in the Galveston area, and for the Corpus Christi region, six more parallel tracks were selected.

The properties for the storm size (Rp) and intensities (cp) were specified based on the investigation of the discrete data set of Irish and Resio. (2009). While the storm tracks were somewhat densely placed in order to capture the effect of spatial variability in continental shelf width, if any, subsets for storm size and intensity combinations were alternately applied for each track to optimize numerical simulation requirements. That is, if the subset for the first, third, and fifth track, respectively, near Galveston, consists of at least nine different combinations of size and intensity properties (subset I), the second and the fourth tracks were specified with combinations of only two discrete intensities (960mb and 900mb) and a single moderate size (subset II) (see Fig. 21). Table 3 lists the combinations of storm size and intensity selected for subset I and subset II,

respectively. On the basis of these two setups, synthetic hurricane wind fields were created with intensity between 960mb and 900mbs, and size between 11 and 65km.

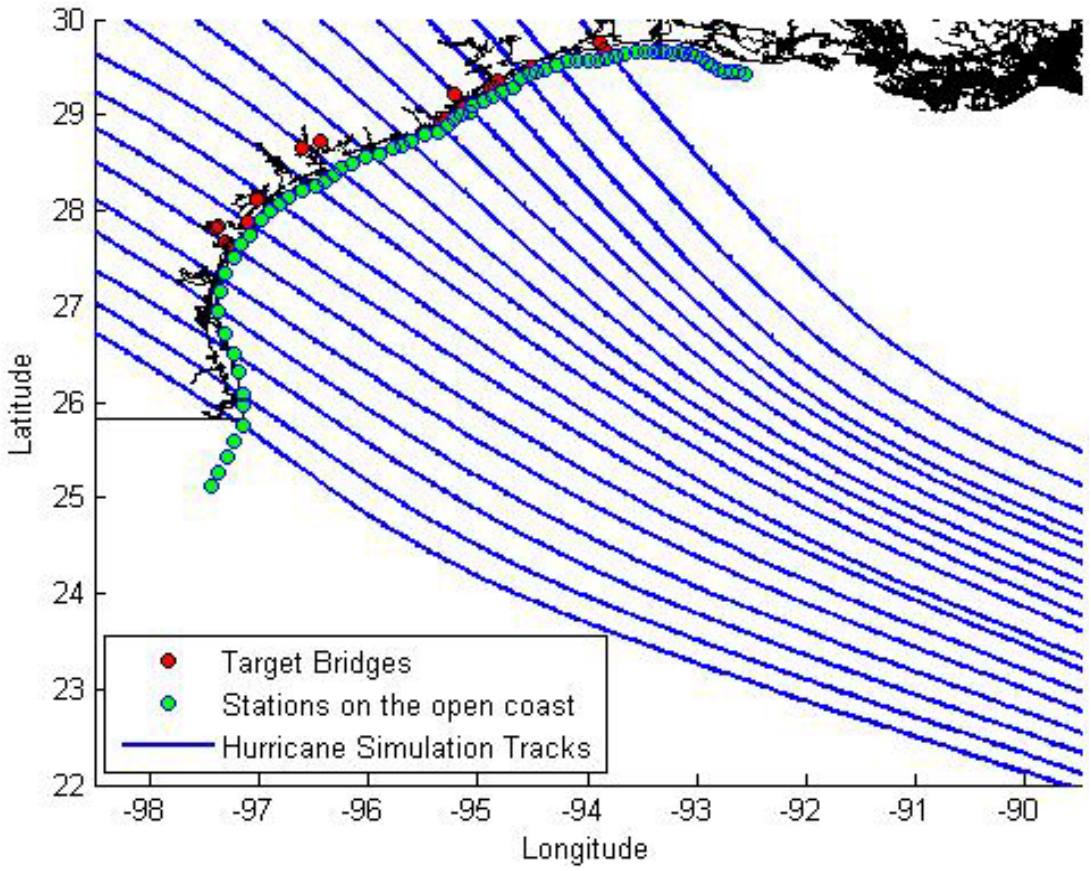

Fig. 20 Storm tracks (solid line) with respect to stations along the Texas coast. The green dots aligned along the shoreline represent the elevation stations while red dots indicate target bridges.

As mentioned previously, the computation of barometric pressures and wind velocities were specified every 900 seconds and saved in two separate files in a format compatible to ADCIRC model specification. With these wind field files as meteorological forcing input, along with the other inputs for grid and boundary conditions, more than 105 ADCIRC hurricane simulations were conducted. With the

refined grid, approximately 1300 CPU hours were requested to complete a single run for a storm of 6 days duration with 0.5 second time increment. To alleviate the computational burden, in terms of time and facilities available, the simulations were run on multiple processors (32, 64, 72, or 88), depending on platform and parallel configuration of the computational platform. The ADCRIC computation produced the time history of the storm surges with the typical accuracy of 20 to 30 cm (Westerink et al., 2008).

Table 3. *Rp* and c_p Combinations for subset I & II

Subset I				
x_{eye} [Lon.]	y_{eye} [Lat.]	v_f [km/s]	c_p [mb]	R_p [km]
-95.65	28.75	5.7	960	20.4
-95.65	28.75	5.7	960	38.9
-95.65	28.75	5.7	960	66.0
-95.65	28.75	5.7	930	14.8
-95.65	28.75	5.7	930	32.8
-95.65	28.75	5.7	930	47.8
-95.65	28.75	5.7	900	11.1
-95.65	28.75	5.7	900	27.6
-95.65	28.75	5.7	900	40.4

Subset II				
x_{eye} [Lon.]	y_{eye} [Lat.]	v_f [km/s]	c_p [mb]	R_p [km]
-95.35	28.90	5.7	960	32.8
-95.35	28.90	5.7	900	32.8

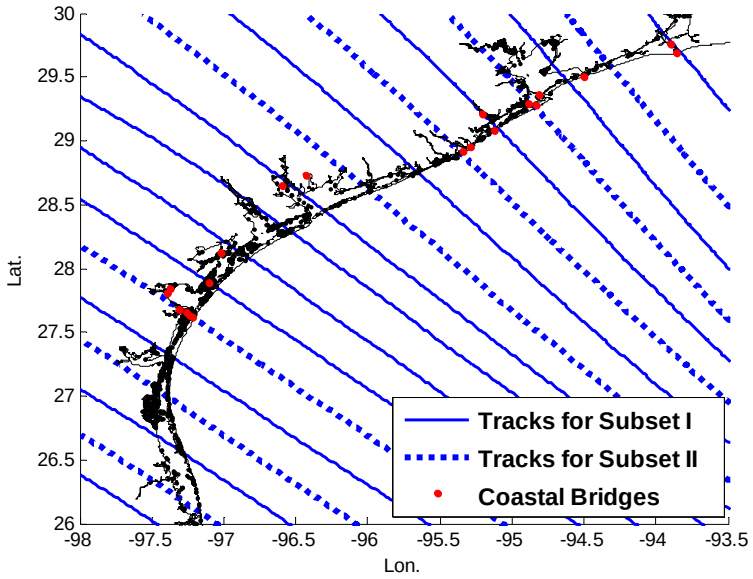

Fig. 21 Tracks for subset I & II. The solid lines are the tracks for hurricane simulations for subset I consisting of minimum 9 combinations of Rp and Cp. The dashed lines are the tracks for hurricane simulations for subset II consisting of minimum 2 combinations of Rp and Cp as shown in XXXTable 3

CHAPTER VI

EXTREME SURGE ESTIMATION USING SURGE RESPONSE FUNCTION

6.1 Surge Response Function Advancements

The storm simulation data was analyzed to determine the dimensionless SRF parameters based on the physical scaling laws of Irish et al. (2009), and then refined to account for continental shelf width

First, the effect of varying coastline configuration on the spatial extent of storms peak surges was studied. As discussed in section 4.3, the location of the peak surge should be analyzed in relation with the continental shelf width, or L_{30}. To measure the L_{30}, several pairs of two ocean stations were specified to locate at the 10m and 30m water depth, respectively, on the virtual orthogonal to shoreline orientation. Alongshore distance between two 10m depth stations were set with simulated hurricane landfall spacing, which is 30km (Fig. 22). To measure the alongshore peak surge distance (x-x_{peak}), however, a minimum of nine combinations of storm surge results along the 10 tracks were utilized (Fig. 23). The size parameter λ was determined from surge data simulated throughout the Texas coast, as a means to account the effect of varying L_{30} for the SRF. By linear regression, the relationship between L30 and the alongshore extent to highest surge was investigated, with respect to the storm size. The increase in steepness of the linear interpolation (or λ) with wider L_{30} and increasing storm size (R_P) resulted from the analysis (Fig. 24). Therefore, it was concluded that the simplification of slowly

varying coastal geography was not valid for SRF development within the wide range of conditions seen on the Texas coast.

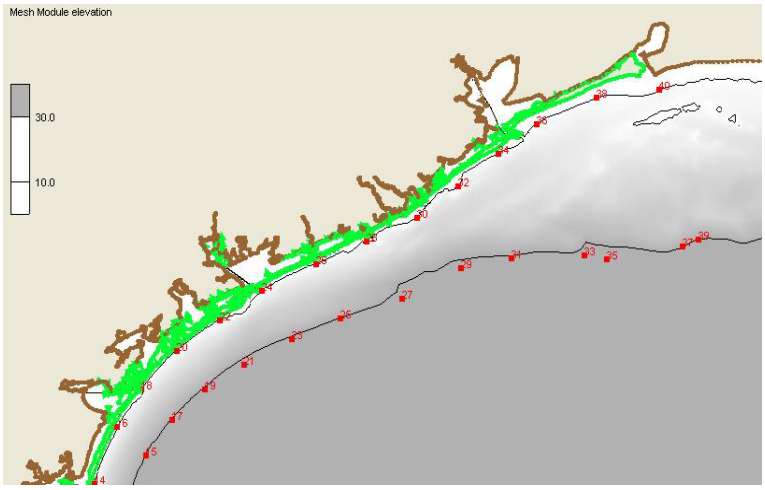

Fig. 22 Locations of 10m and 30m water depth on the continental shelf. A pair of two depth indicators were specified on virtual orthogonal line with respect to shoreline orientation to measure L30

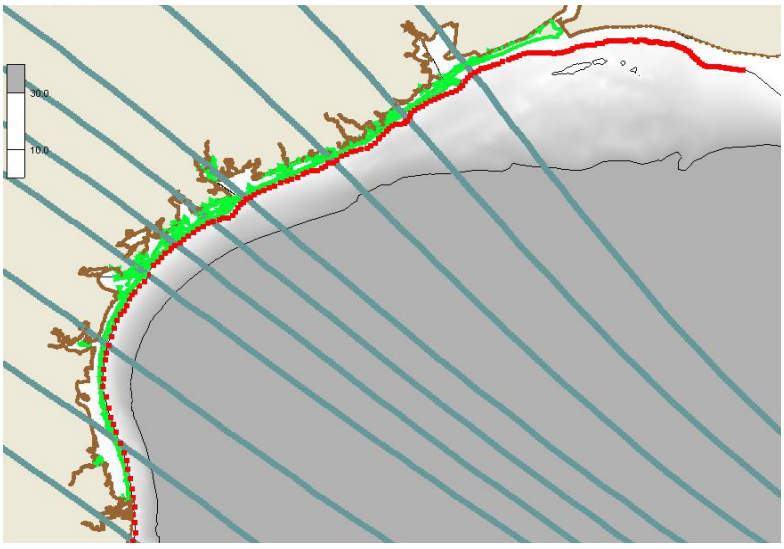

Fig. 23 Hurricane tracks selected (green solid lines) to measure the effect of varying continental shelf width (L30). From the bottom left across the top right, track 1, 3, 5, 7, 8, 9, 10, 12, 14, 16, and 17, respectively. The solid line in black marks the 30m water depth contour while the red dots represent the elevation stations specified at 10m- water depth in the coast.

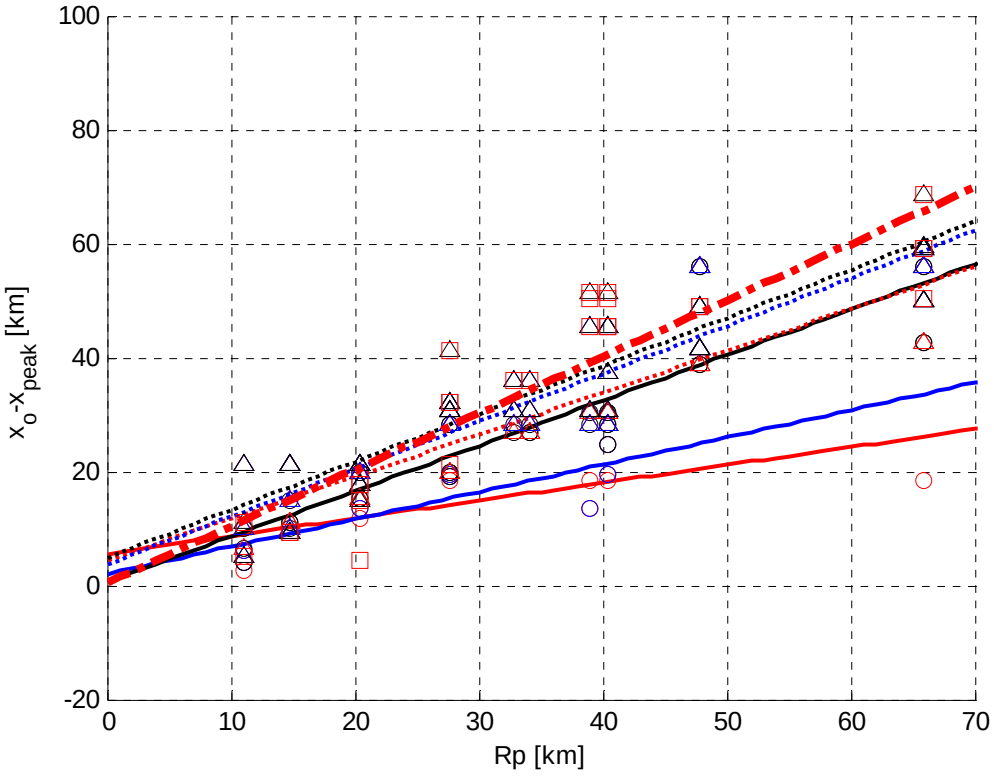

Fig. 24 Linear regression of storm size (Rp) and the distance between the location of hurricane eye at landfall and the alongshore peak surge location. The slope of each interpolation is used to determine t the slope parameter, λ.

To incorporate the different geographical conditions, the total study area was divided into three parts depend on the variability in the parameter λ (

Table 4); the coastal regions near Corpus Christi, Matagorda Bay, and Galveston, respectively. By partitioning the continuous coastal regions into three spatial ranges, the previously used simplification of slowly varying coastal configuration is then applicable within each segment of the coast (i.e., Galveston, Matagorda Bay, and Corpus Christi).

Table 4. Properties of the parameter λ for each segmentation of the Texas coastal region

Selection of λ and storm tracks applied for each study area		
Coastal Region	λ	Track I.D.
Corpus Christi	0.74	5,7,8,9
Matagorda Bay	0.84	7,8,9,10,12
Galveston	0.99	10,12,14

Table 5 lists the variation in λ estimated from storms propagating over the corresponding L30. These were plotted in Fig. 25. This figure shows that the distribution of the λ with respect to varying L30 can be categorized into three groups depending on their slopes – the magnitude of increase in the λ with uniform variation in L30. If we visualize the range of the continental shelves classified in the same group on the continental shelf map (Fig. 25), it is seen that the overall geography of the continental shelf shape along the Texas coast can be divided into three segments (Fig. 26, separated with the solid lines) based on the lambda variation.

In addition to the correlation between L30 and λ, it is seen that the lambda variations also corresponded to the changes in the shoreline orientation. Therefore, it is expected that, by examining the correlation between L30, Rp, parameter λ, and the shoreline orientation θf, the SRF could also provide a means to characterizing the regional geographical features in parametric function. Meanwhile, the effects of such a varying costal shape can be resolved by assuming that the interaction between the hurricane meteorology and the geographical factors in the region can be captured by the surge responses to the hurricanes approaching the vicinity of the area of interest. Therefore, when determining the site-dependent coefficients, such as λ and mx,

reflecting the regional characteristics, storm simulation results from selectively chosen tracks were only utilized. For example, for the evaluation of λ and mx for bridges located in the Corpus Christi area, the storm surge data obtained from storms simulated along the track No.5 to No. 9, and in-betweens was only used.

Table 5. Lambda variation change in the continental shelf width

3 - pair		
Track ID	L30 [km]	Lambda
1,2,3	19.6	0.26
2,3,4	20.6	0.36
3,4,5	21.3	0.49
4,5,6	23.5	0.70
5,6,7	25.4	0.69
6,7,8	28.0	0.79
7,8,9	30.1	0.74
8,9,10	33.1	0.84
9,10,11	35.7	0.81
10,11,12	39.5	1.01
11,12,13	41.7	1.12
12,13,14	47.9	1.01

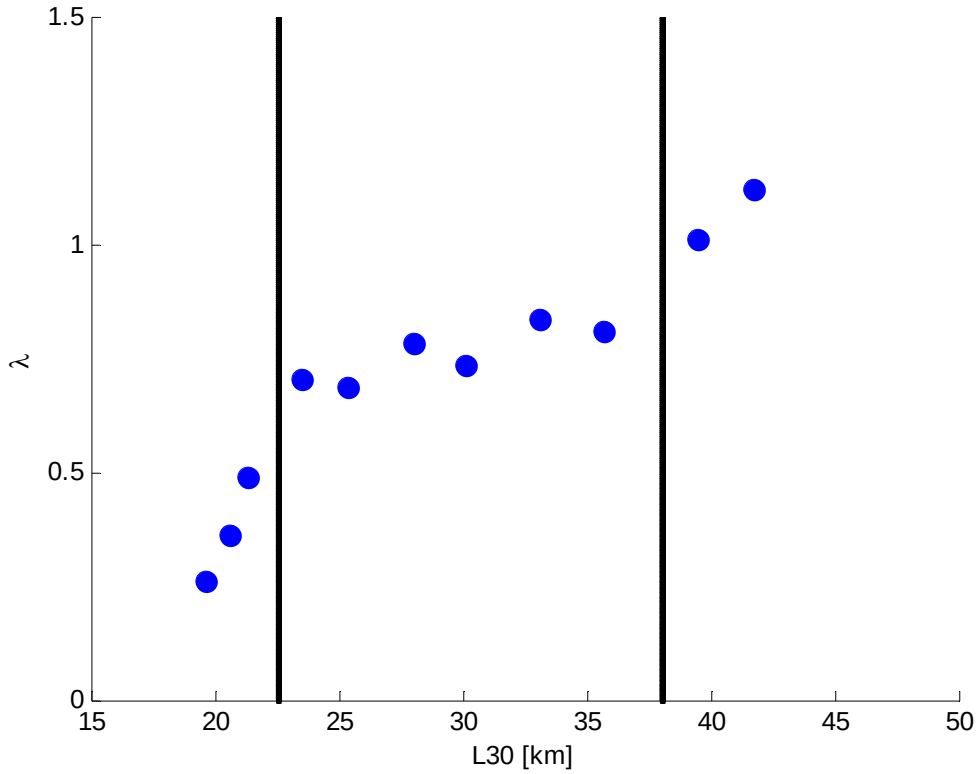

Fig. 25 The parameter λ variations with respect to varying continental shelf width. The solid lines separate the research area into three segments.

Fig. 26 Continental shelf map of the Texas coast. The dark shade represents the continental shelf extension to the 30m water depth (L30). The red box represents the alongshore range of L30 within which the parameter λ shows the similar tendency in the distribution with respect to L30.

The properties for λ, along with the surge simulation data, were used to determine the dimensionless SRF parameters (x2' and ζ') following the methods presented the previous sections. The obtained sets of x2' and ζ', were curve-fitted. As a conclusion, the flexibility of the three-term Gaussian function in adjusting peak width was found to be the most suitable for defining the SRF, as applied during previous preceding work by Irish et al. (2009). However, the region to the right side of the hurricane eye is the most influenced by the hurricane forcing, due to the hurricane meteorology in the northern hemisphere. Therefore, SRF behavior has some asymmetry with respect to x2'=0. In an effort to find a way to improve the flexibility in the shape of the function, two pairs of three-term Gaussian functions were defined based on the right and left side of the data, independently. In this way, the scatter near the peak of SRF was minimized, and thus a smoother curve, with its peak well-posed at the center (the location of x2'=0), could be developed. This curve fitting approach also reflects the asymmetry of the surge behavior. Therefore, the SRF near the 20 selected bridge locations were developed in a format of an asymmetric three-term Gaussian function.

As discussed before, the SRF is a site-dependent function. Therefore, for the 20 target bridges, 20 independent SRFs were developed. The SRFs for each bridge are presented in the Appendix, and three of these SRFs are presented here for discussion (Fig. 27).

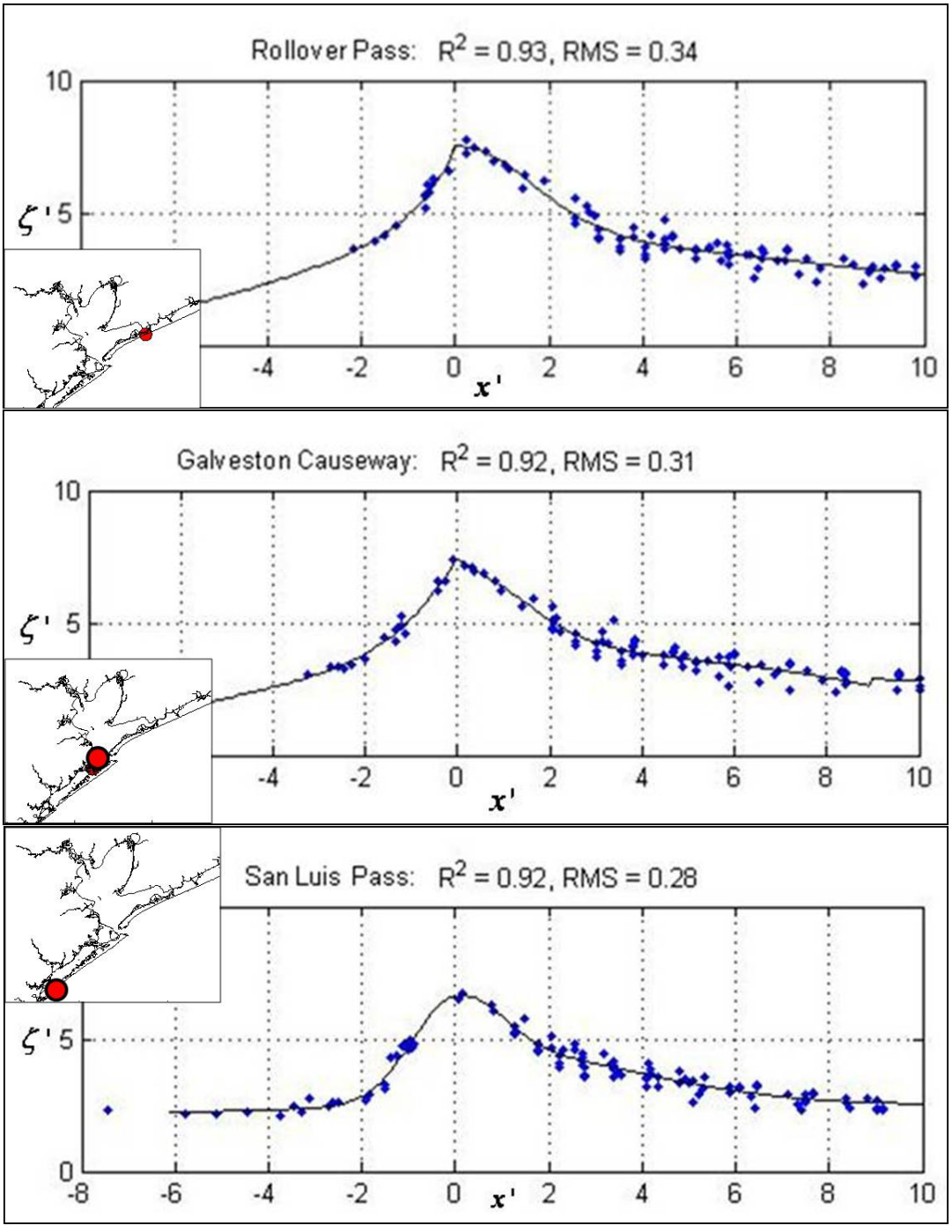

Fig. 27 Surge response functions developed at the three locations in Galveston. The SRFS are developed at the location of Rollover Pass(top), Galveston Causeway (middle), and San Luis Pass (bottom). Solid line represents the three-term Gaussian fit to the data.

6.2 Validation and Justification of the Surge Response Function Methodology for Hurricane Flood Probability Analysis

By comparing the surge predictions made by SRFs to the original numerical simulation output, the accuracy of each SRF could be estimated. Since the SRF is a developed by the data-fit function of the dimensionless parameters, inherently the SRF itself is a dimensionless, continuous function of the hurricane parameters. Therefore, with given hurricane conditions, the SRF provides the general use of itself for predition of dimensional surges by back-calculating from the SRF.

The SRF was used in this way to make predictions of storm surges (ζsrf) based on the hurricane conditions applied for generating synthetic wind fields earlier as forcing input for storm surge simulations (ζsim). Using the SRFs presented inFig. 27, the SRF predictions (ζsrf) were compared to the ADCIRC model simulation results (ζsim), as shown in Fig. 28. The solid line crossing on the center represents an exact match between the two results.

At the elevation stations on the open coast, the root mean square errors (RMS) of (ζsrf – ζsim) were estimated to be between 15cm and 32cm. This is consistent with the results resulted by Irish et al. (2009). Considering the accumulative errors due to model computation capability is the order of 20 to 30 cm (U.S. Army Corps of Engineers, 2006), the magnitude of RMS errors between the two predictions is reasonable. Therefore, we concluded that the obtained SRFs for the 20 bridge locations of interest accurately represent the surge behavior along the Texas coast.

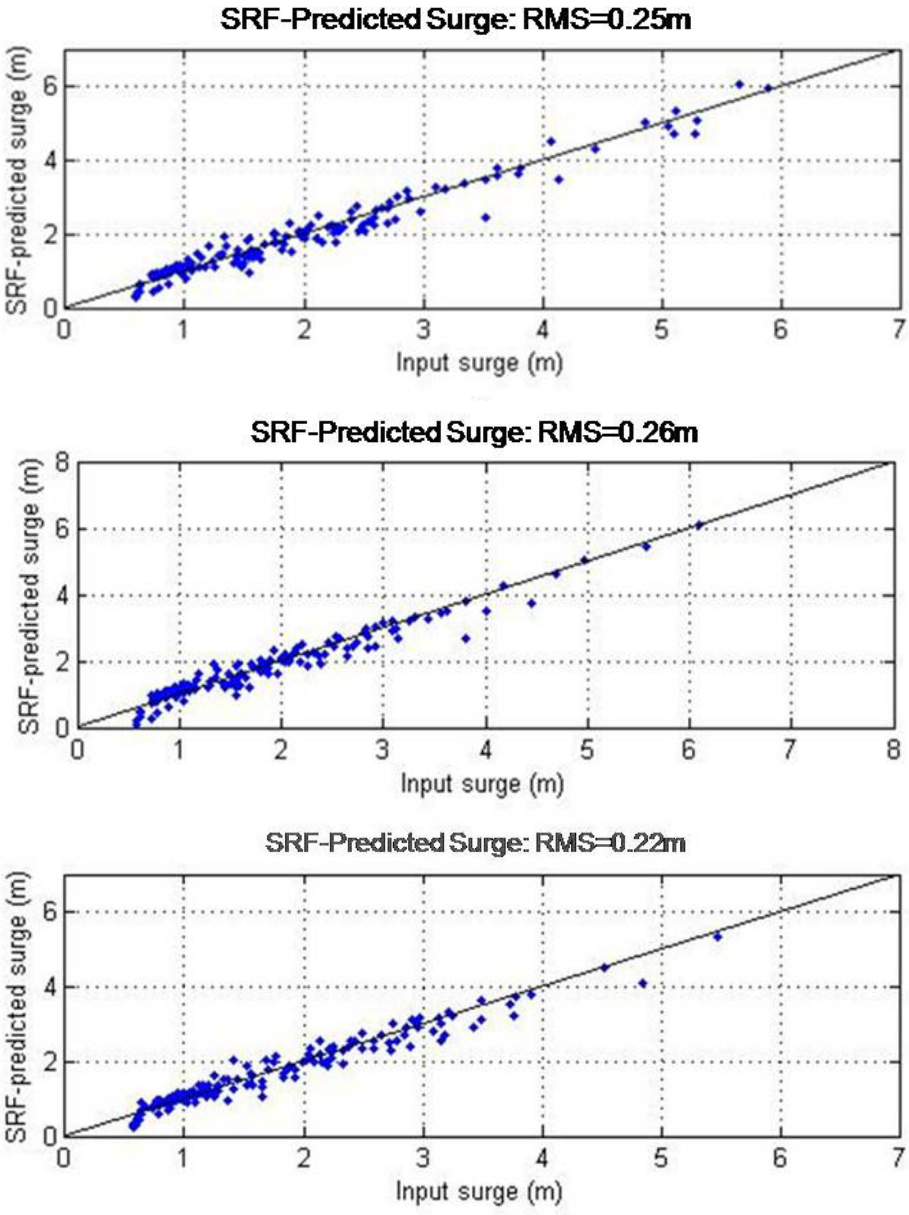

Fig. 28 ζsrf - ζsim plots. The values on the vertical axis are SRF surge predictions while those on the horizontal axis are ADCIRC surge simulation results. Rollover Pass(top), Galveston Causeway (middle), and San Luis Pass (bottom). Solid line indicates the exact match.

To better optimize SRF performance, further study on the interaction between surges and the bay site environment is in process (Katyal, Personal communications).

Note that all surge levels predicted by the SRFs are based on the surge data computed from the numerical model. During ADCIRC simulations, only the hurricane wind stress and pressure forcing forced the surge. Therefore, these SRFs do not account for additional water level due to wave radiation, astronomical tide, and surface water runoff. Finally, static topography within the ADCIRC model was employed, so any additive flooding due to lowering of the barrier islands during the storm is not included.

CHAPTER VII

APPLICATION OF SURGE RESPONSE FUNCTION FOR PEAK SURGE ESTIMATION

By virtue of its continuous form across hurricane meteorological parameters, the SRF can be utilized to calculate storm surge levels at given locations for any hurricane, once the properties for storm size, intensity, and the distance from a point of interest to the hurricane eye at landfall are known. For extreme surge analysis, the SRF was developed based on the peak surges extracted from the entire surface water level history from each ADCIRC simulation. Therefore, the surge prediction made by SRFs may be considered to be the peak surge level at that location for the given hurricane meteorology.

To demonstrate and validate the use of the SRF methodology, storm surge predictions for two historical hurricanes (Carla (1961) and Ike (2008)) were carried out. The SRF-predicted surge levels were compared to high water marks (HWMs) and water level gauge measurement taken during and after these hurricane events.

The focus of this study is on evaluating the extreme surge level response against the hurricane forcing represented by the surface wind stress, pressure deficit, and their interaction with the local bathymetry. Flood levels derived by other forcing mechanisms were not included in the surges predicted by SRF, but it is noted that processes including wave setup and tides can contribute substantially to overall flood elevation. Thus, when the SRF predictions are compared to observations, some of the differences between the two water levels were anticipated and can be attributed to the effects of wave setup, astronomical tide, land erosion, and runoff. For example, the wave setup contributes

approximately 10 to 20% of the total flood level at the open coast. In addition, there is inherently uncertainty with HWM data, due to the nature of its collection with respect to debris lines, visual observations, and so forth. Moreover, it has to be noted that HWMs often include individual wave runup.

For comparison between the SRF predicted peak surges and the Hurricane Carla observation, the HWMs as given by debris or drift lines on the buildings were used. The HWMs were measured with respect to the Geodetic Vertical Datum (NGVD29), while the SRF predictions were made with respect to MSL. The HWM data were converted to MSL using datum information for the 1983-2001 tidal epoch. This conversion gives MSL to be higher than NGVD29 by about 0.2m in the vicinity of the Galveston and 0.3m in the vicinity of Corpus Christi, based on the benchmark information for the NOAA Galveston Pier 21 and the NOAA Rockport, respectively.

For the comparison between the SRF predicted peak surges with the Hurricane Ike high water levels, peak observed water levels computed from the time history collected with pressure gauges were used. The water level time series were obtained from pressure gauges deployed by U.S. Geological survey (USGS, 2005 and 2008) prior to Hurricane Ike's passage. The water level data used for comparison were measured with respect to North America Vertical Datum (NAVD) of 1988. To make it comparable with SRF prediction, these data were converted to MSL. The benchmark data indicate MSL is higher than NAVD88, about 0.35 m.

7.1 Hurricane Carla Description

Hurricane Carla was one of the most powerful hurricanes seen in the United States hurricane record, especially for the state of Texas. Hurricane Carla was first classified as a hurricane as it passed through the western Caribbean Sea on September 6, 1961, and this storm steadily evolved to a Category 5 hurricane while approaching the Texas coast in Gulf of Mexico (Fig. 29). At its landfall on September 11, 1961, between Port O'Connor and Port Lavaca in Texas, Carla was a Category 4 hurricane with a lowest pressure of 931mb, maximum sustain wind speed of 64 m/s, and radius to maximum wind of 56km (NOAA, 2009) As it was a large and intense hurricane moving slowly, at 1.8 m/s, a wide span of the Texas coast, from Port Lavaca to Galveston, experienced some of the highest storm surges ever recorded in this area, 3.3-3.7m (NOAA unknown)

7.2 Comparison of the Peak Surges from Surge Response Function Predictions with High Water Mark Observations

Using the hurricane parameters for Hurricane Carla, SRF predictions were made and compared to the HWMs published by NOAA (1982). The peak storm surge levels evaluated from SRF prediction and observed from the HWMs, with respect to MSL, are listed in Table 6. In addition, the surge levels listed in this table are also plotted on the same graph (Fig. 30) in order to visualize the comparison.

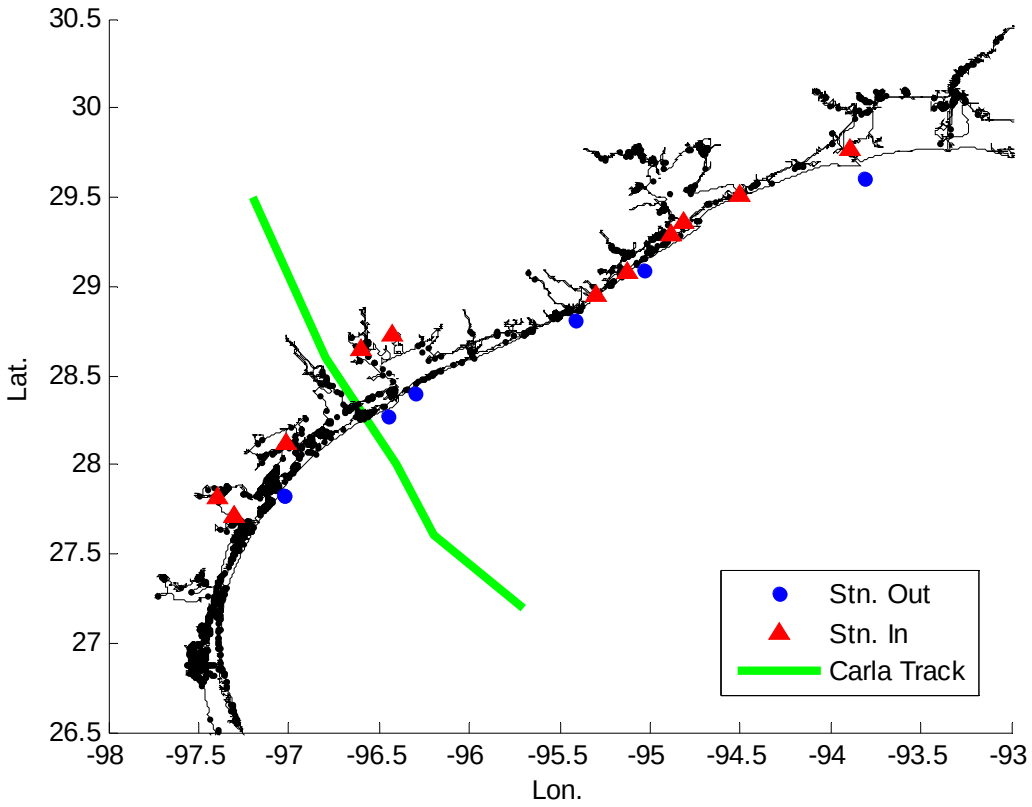

Fig. 29 Hurricane tracking map and elevation stations. SRF prediction was made at stations marked with triangles and compared to the HWM reported by National Weather Service, NOAA (Miller 1982) at the corresponding locations. The solid line shows the Hurricane Carla's storm track* with respect to the elevation stations. *Based on information from National Hurricane Center (2008).

Table 6. Hurricane Carla surge estimation from HWM and SRF

Hurricane Carla Surge Comparison			
Stnation No.	distance from landfall [km]	HWM above MSL [m]	SRF Prediction [m]
51	-43.7	2.8	2.1
53	-41.6	1.6	1.4
58	-30.5	2.6	2.1
65	-16.2	2.0	1.9
77	9.5	3.4	2.5
83	20.6	2.9	2.9
84	20.6	4.5	3.8
88	25.9	5.4	5.2
110	71.2	3.1	3.6
117	80.5	3.7	4.1
127	92.9	3.1	3.8
132	97.0	3.5	3.7
141	111.5	2.5	2.5
147	120.8	2.7	2.6
157	133.5	2.7	3.1
179	164.5	2.5	2.9
182	166.2	2.0	2.1

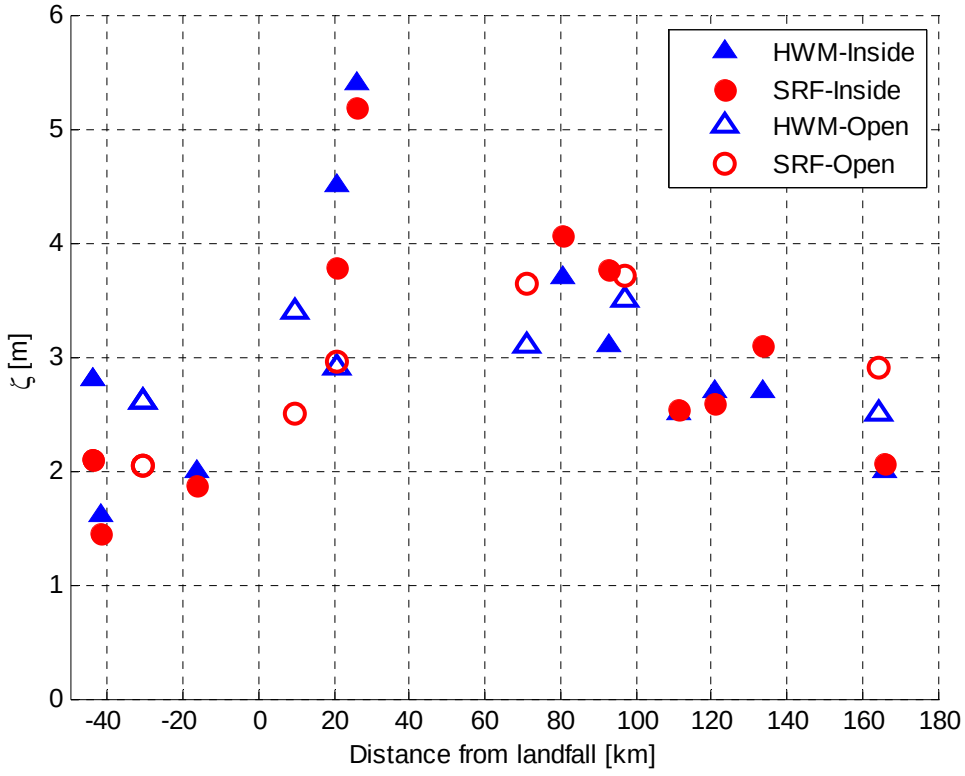

Fig. 30 Comparison of the SRF prediction to HWM for hurricane Carla. Surge levels were estimated with respect to MSL at the elevation stations as shown by Fig. 22.

From the comparison of the two data sets, it was shown that a clear correlation exists between the SRF predictions and the historical HWMs. Based on the pairs of data obtained at 17 stations located inside the coastal bays or along the open coast, the root-mean-square (RMS) error was estimated to be 48 cm, and a strong correlation, with the correlation coefficient of 0.87, between two data sources were found. The SRF predictions only included storm surge by wind and pressure deficit, whereas the HWMs include wave effects (i.e. setup and runup) and astronomical tides. The additional effects of waves and tides were more obvious when comparing the difference in two the surge levels at the stations located on the open coast (hollow marks on Fig. 30) than with

those located inside a coastal bays (solid marks on Fig. 30). Also, the fact that the flood levels recorded through HWM are known to have a high degree of uncertainty leads to differences in two data sources.

7.3 Hurricane Ike Description

On September 13, 2008, while this study was on going, Hurricane Ike struck the Galveston area and caused damage to several coastal bridges and roadways, including the Rollover Pass and Pelican Island Bridges. As Hurricane Ike began moving northwesterly into the Gulf of Mexico, it was upgraded to a Category 4 hurricane. Although Ike's intensity weakened to a Category 2 by the time it made landfall at Galveston, Texas, because of the wide extent of the hurricane force wind field, it resulted in huge storm surges along the Texas coast. Near landfall, the size of the eye was 58km, the center pressure was 952mb, and it approached the coast with speed of 19.3km/hr. With the given Hurricane Ike meteorology, surge predictions were made using the SRFs at several stations located near the eye of Hurricane Ike (Fig. 31). The positions of these SRF stations were specified to correspond to the locations of the pressure monitoring sensors deployed by the USGS prior to Ike's landfall. The SRF predictions were compared to the peak measured water level from the USGS gauges to verify its accuracy.

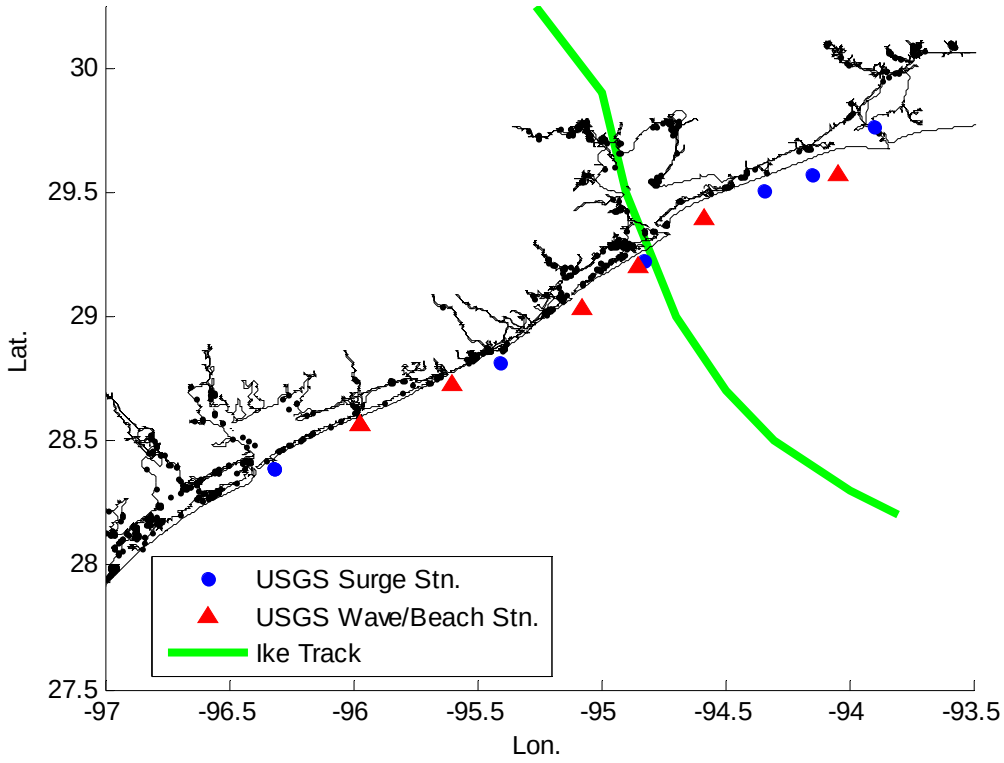

Fig. 31 Hurricane Ike tracking map and elevation stations. SRF prediction was made at stations marked with triangles and compared to the peak water level measured by USGS (2009) at the corresponding locations. The solid line shows the hurricane Ike's storm track* with respect to the elevation stations. ***Based on information from National Hurricane Center.**

7.4 Comparison of the Extreme Surges from SRF Predictions with Peak Water Level Observations

USGS (2009) has classified the site of recording the peak water level either as a surge station (Hollow on Fig. 32), or wave/beach station (Solid on Fig. 32) depending on the gauge configuration at the region. That is, in the surge-type flooding, the observed water level was presumed to have affected solely by the quasi-steady flood levels, including wave setup. On the other hand, some gauges which did not filter surface waves

are classified as a wave/beach type (USGS, 2009). With this discrimination, the surge predictions from the SRFs were compared to the peak water levels at the USGS stations. To examine the alongshore variation in the surge levels, the wave/beach stations located on the open coast were selected. However, at some locations, where the wave/beach stations did not exist nearby, the outer-most surge type stations, located behind barrier islands or in bays, were selected. In this way, the distance between consecutive stations was kept relatively constant. The numerical prediction results are listed in Table 7 and they are plotted in Fig. 32.

The data comparison shows a strong correlation, with a correlation coefficient 0.93, between the SRF values and the USGS measurements. Although the RMS for the 12 measurements is 75 cm, this was anticipated since the SRF predictions did not include the effect of wave setup or tides. However, since the effect of wave setup is smaller behind the barrier islands, much smaller differences between the SRF prediction and the surge-type flood levels are seen in; here, RMS error is 43 cm. Additionally, larger gaps between two sets of data and more scattering in USGS data are seen in the data distribution at the east side of Galveston, compared to that at the west side of stations. Considering the SRF prediction still shows consistency in surge level trend, the increase of inconsistency between SRF predictions and USGS observations near and on the right side of the location of the hurricane landfall can be explained by the effect of the changes in geographical features such as lowering of barrier islands due to relatively stronger hurricane impact in the east part of Galveston.

Table 7. Hurricane Ike surge estimation from peak surges and SRF

Hurricane Ike Surge Predictions			
Station No.	SRF Prediction [ft]	HWM above MSL [m]	SRF Prediction [m]
82	3.0	1.2	0.9
94	2.4	1.2	0.7
105	5.1	2.6	1.6
110	6.3	1.5	1.9
126	8.7	2.7	2.7
138	9.0	4.2	2.7
139	9.8	3.6	3.0
151	13.1	5.6	4.0
161	14.5	4.7	4.4
167	16.3	4.9	5.0
170	16.5	5.4	5.0
182	11.2	3.0	3.4

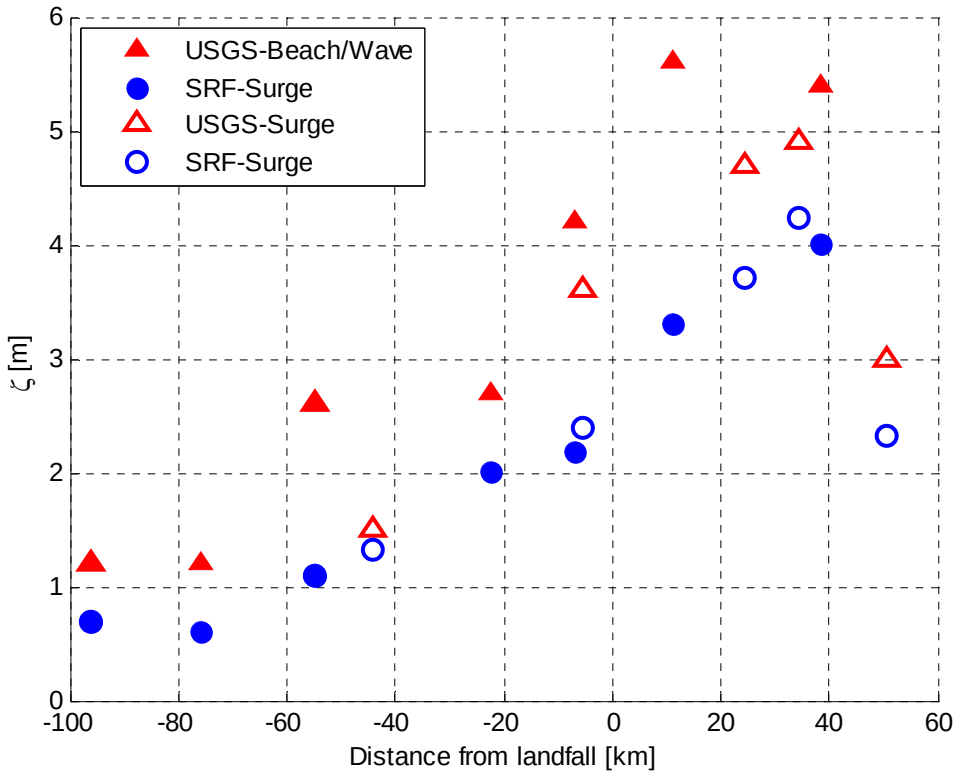

Fig. 32 Comparison of the SRF prediction to peak water level record during Hurricane Ike. Surge levels were estimated with respect to MSL at the elevation stations as shown by Fig. 18.

7.5 Discussion of the Comparisons

The two sets of comparisons between the SRF predictions and field measurements demonstrated the performance of the SRF in capturing the surge response trends with alongshore spatial changes. In particular, the information on the spatial variation in storm surge levels, produced by the SRFs, can be used in predicting the maximum flooding suspected location, along with the peak surge levels at that location.

Furthermore, the surge response predicted using several SRFs for a given hurricane condition showed a clear correlation with the observed data for both hurricanes considered. Owing to the SRF methods ability to utilize any set of hurricane

meteorological conditions by turning into the dimensionless input into a dimensionless surge, the study of two hurricanes with different meteorological conditions, making landfall at two different locations along the Texas coast, proved that the SRF can be applied for accurate storm surge predictions over a wide range of hurricane conditions.

On the other hand, as the SRF method presented here was developoed to predict the storm surge behavior with respect to the hurricane wind and pressure fields, the storm surge predictions made by these SRFs do not include the the additional surge generated by wave breaking (wave setup),), astronomical tides, and additional flooding induced by changes to geographical features (dune slope change and lowering of the barrier island) during the hurricane events. The exclusion of these factors in the SRFs, in addition to potential errors in the field measurements thhemselves, introduces a bias between the SRF predictions and the observed data., particularly along the open coast. However, even with the expected bias, the alongshore distributions between two sets of data showed strong correlation. That is to say, the difference in flood levels between two sources of data can be justified by the factors mentioned above. While the SRF method is based on parameterized meteorology, which does not account for natural variability in the hurricane wind field, for example, the relatively good correlation between the SRF predictions and the measurements gives a strong indication that the SRF method is robust enough for general application.

CHAPTER VIII

APPLICATION OF SURGE RESPONSE FUNCTION METHOD FOR FLOOD PROBABILITY ESTIMATION

In this thesis, the water surface response against hurricane meteorology was predicted through the SRF method at twenty Texas coastal bridges. Besides its capability to predict the surge levels for given hurricane conditions, the SRF method has further potential to be applied for flood probability analysis.

If we can specify the possible range of the properties for these hurricane meteorological parameters at a location of interest- in this study, a coastal region in the Gulf of Mexico. Since the SRF is represented by a continuous function with respect to dimensionless parameters based on scaled hurricane meteorological parameters, a set of any given properties for each hurricane parameter can be used as input to the SRF. Therefore, the sets of possible properties for the hurricane meteorology in a region can be converted to form the input sets for SRF. Consequently, the peak surge elevations corresponding to the combination of the hurricane properties can be estimated from the SRF.

For illustration, if we consider the possible range of intensities and sizes in the Gulf of Mexico to be from 870mb - a Maximum Potential tropical cyclone Intensity (MPI, Tonkin et al., 2000) - to 960mb and as from 8km to 120 km, respectively. In addition, if we further assume that we are interested in the surge flood levels generated from storms making landfall with 200km of the location of interest. Using the SRFs

developed earlier, the peak surge levels over this range of conditions can be calculated at the intersection of each $R_{p,}$ c_p, and x_o set. The surge response surface generated for selected conditions are represented the panel of Fig. 33. Notice that the vertical heights of any points on the surface represent the surge levels estimated based on given conditions. Therefore, the surge response surface represents all possible flood levels due to the entire hurricane meteorology range considered (Fig. 34). One should notice that the crest of each surge response surface represents the optimal hurricane condition for generating the highest surges. That is, for a given set of R_p and c_p, the SRF developed at an arbitrary location of interest provides the information on the potential location at which the maximum hurricane flooding takes place, as well as the peak surge level at the location. For extreme-value analysis, it is useful to identify the maximum possible hurricane anticipated at a location of interest, as this will specify an upper bound to the stage-frequency (water-level vs. return period) distribution. This is strength of the JPM-OS; since a logical upper limit on hurricane intensity exists, the MPI, a maximum possible surge can be identified. To demonstrate the use of the SRF for identifying this upper limit, the maximum possible surge levels were calculated at all three bridge locations based on the SRFs presented in the previous section (Table 8).

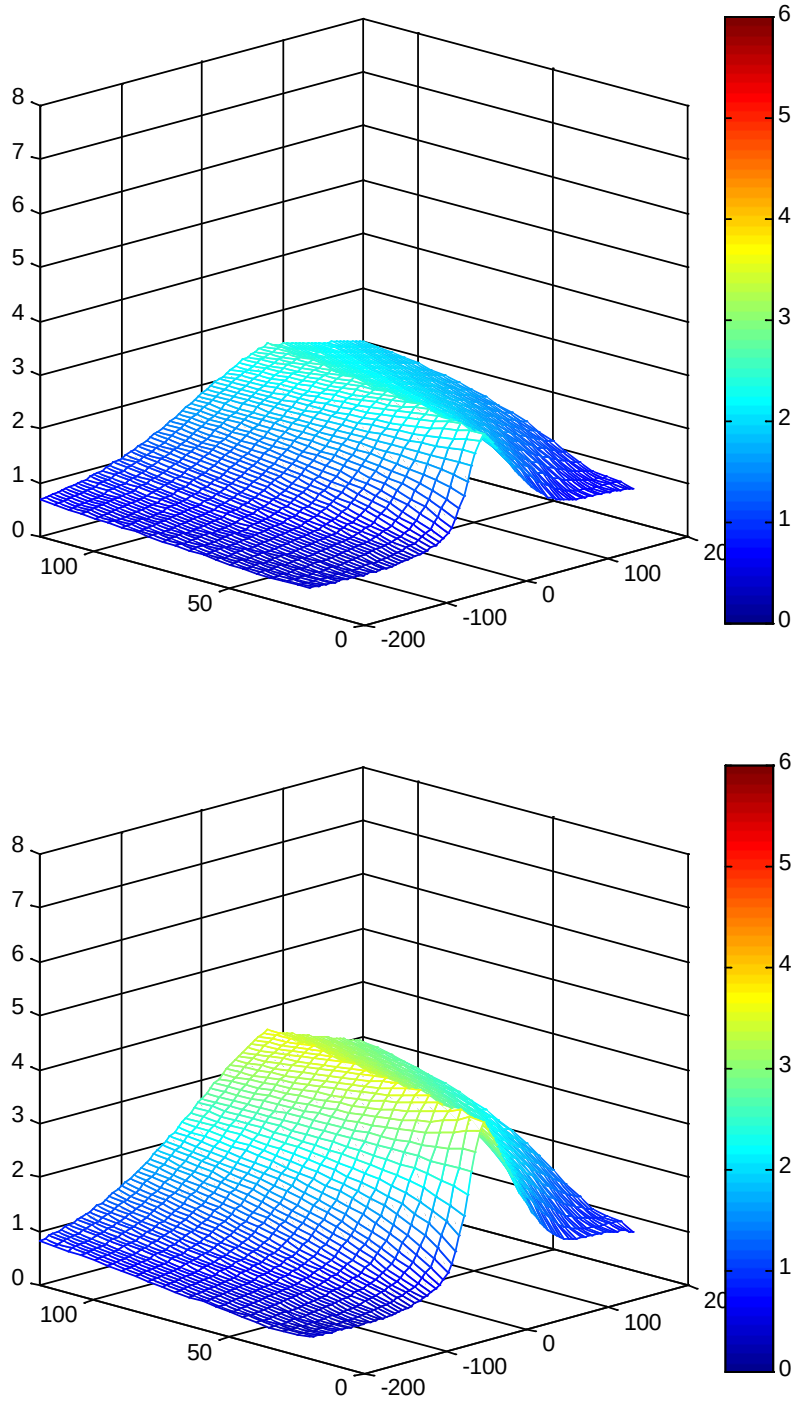

Fig. 33 Surge response surface estimated with respect to the variation of Rp and xo at a fixed location. The surge response surfaces were generated from the storm of cp=960 mb, cp=930 mb, cp=900 mb, and cp=870 mb from the top to the bottom.

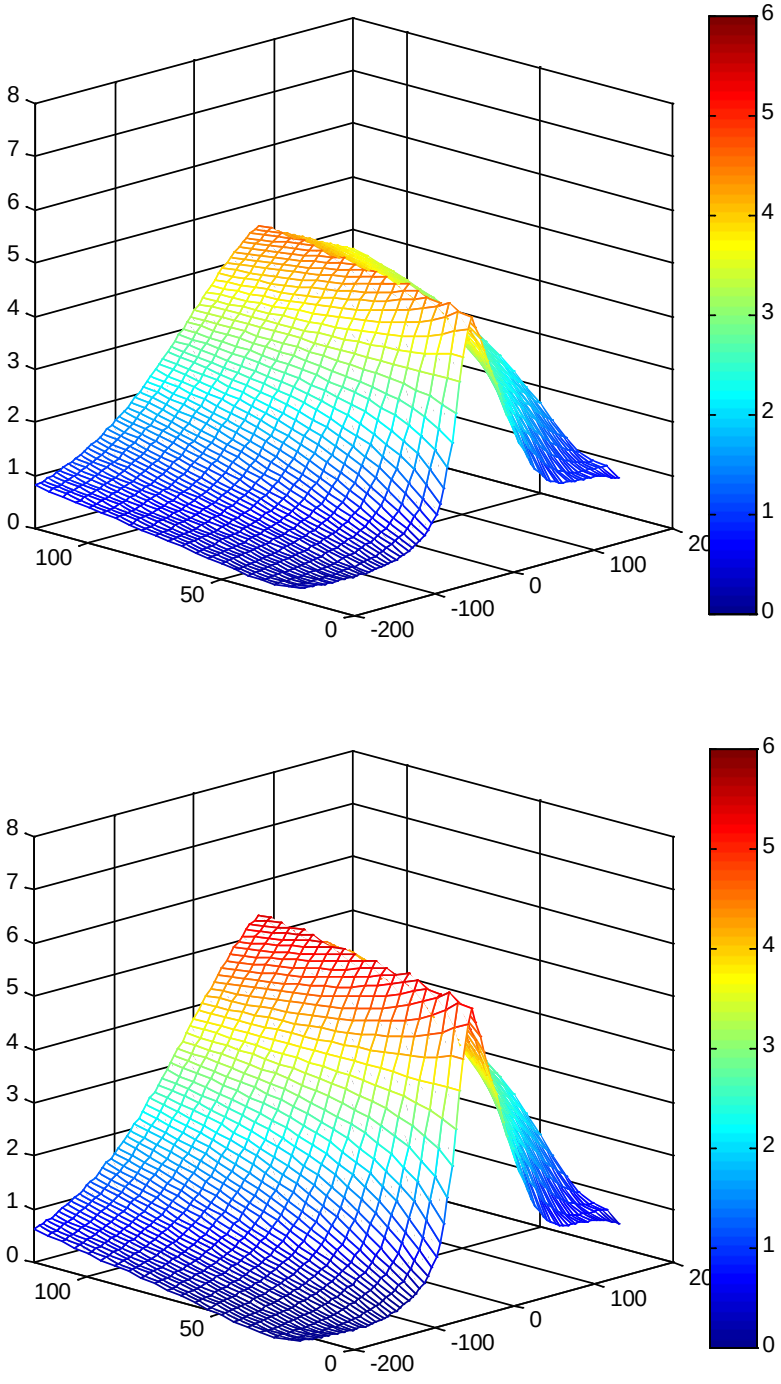

Fig. 33 Continued.

Table 8 SRF extreme surge predictions at three bridges in Galveston

Bridges	ζ_{max} [m]	c_p † [mb]	R_p †† [km]	Peak dist.** [km]
San Luis Pass	6.7	870	50	47.5
Galveston Causeway	5.0	870	116	110
Rollover Pass	7.2	870	44	30

*** ζ =Peak surge level due to hurricane of given intensity and size**

**** Peak dist. =Distance between the bridge and the hurricane ladfall that results in the maximum storm surge at the bridge**

† c_p = Center pressure of the hurricane, in millibar

†† R_p = Radius (size) of the hurricane

The SRF can be utilized for assuming flood probability over a full range of hurricane possibilities, in combination with the JPM-OS. According to the JPM-OS method, the storm surge level at a location of interest can be evaluated by the joint probability of the optimally selected meteorological parameters (refer to Eqn. 4.5). Niedoroda et al. (2007 and 2008) described application of the JPM-OS for the flood probability through the documentation of the Mississippi Coastal Flooding Hazard project. Based on a wide review of the history of hurricane meteorology and a series of 228 hurricane simulations, Neidoroda et al. (2007) produced the statistical estimation of hurricane surge frequencies and flood level distributions over the coastal regions in Mississippi.

The methodology applied by Niedoroda et al. (2007 and 2008) can be modified to suit the flood probability analysis for wide range of coastal regions along the entire

Texas coast, using the SRF. The approach may be developed from the idea that we may use the SRF developed previously, along with the statistical joint probabilities between the size (Rp), intensity (cp), and the relative distance from the eye of storm landfall to a location of interest (xo).

The total range of surge elevation depicted in Fig. 34 can be discretized into several infinitesimal bins representing each elevation range. Since the surface in Fig. 34 represents all possible flood levels anticipated from the hurricane meteorology of consideration, by associating each point on the response surface into corresponding bins of elevation range, the total surge response surface is now transformed to a probability density function for surge. Therefore, with the optimally sampled input properties of the major hurricane meteorological parameters, the flood level statistics can be determined.

Furthermore, the SRF involves site-dependent parameters such as the size parameter λ and intensity slope mx, as studied previously. These parameters are what determine the shape of surge distribution at a specific location. Therefore, the SRF defined at a region of interest, such as the location of one of the coastal bridges along the Texas coast, provides a means for analyzing the storm surge frequencies that reflect both the meteorological conditions and geographical features.

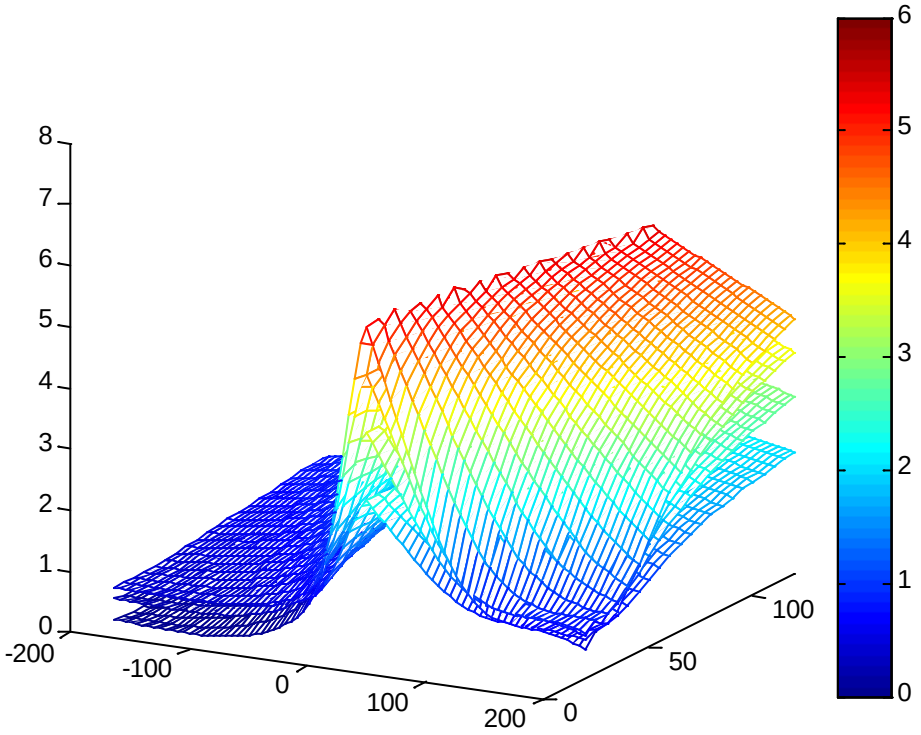

Fig. 34 Combined surge response surface. A function of R_p, c_p and x_o, with respect to a fixed location determines the continuous surge response surface. The surge response surfaces from the storm of c_p=960 mb, c_p=930 mb, c_p=900 mb, and c_p=870 mb on Fig. 33 are accumulated.

CHAPTER IX

SUMMARY AND DISCUSSION

As a course of work to examine the hurricane impact on the Texas coastal bridges against the, first, the flood level derived by hurricane meteorology was estimated near the location of twenty vulnerable bridges widely spread throughout the Texas coast. To incorporate the wide range of study area with minimum computational work load, the SRF method was optimized to use for accurate surge predictions. Based on the numerical storm surge simulations of more than 105 storms traveling over 15 parallel tracks, the twenty SRFs were developed to characterize the storm surge behavior at each target bridge location in the Texas coast. The SRFs performed the surge prediction within 30cm RMS error range, in comparison to the numerically simulated surge levels. Considering the model computation capability is the order of 20 to 30cm, it was concluded that the obtained SRFs were capable of providing accurate surge prediction in the reason of interest.

The capability of the SRF in capturing the spatial trends in storm surge responses on a given hurricane conditions was proved through comparison to the historical storm surge records (Carla, 1961 and Ike, 2008). In addition, the application of SRF for the extreme-value analysis was demonstrated. The peak surge levels expected in the area of the bridge locations were estimated on the various hurricane conditions assumed based on the hurricane meteorology typically observed in the region of Gulf of Mexico. From this analysis, it was shown that the SRF can be used for predicting the relative distance

between the hurricane landfall and the location of the maximum flooding expected on the given hurricane meteorology, as well as the peak surge levels.

The scope of this study was to optimize the use of SRF to produce the peak surge predictions on the various hurricane meteorological conditions over wide range of the Texas coast. During the overall study, the effects of the varying shoreline orientation, sensitive to the storm forward speed, and the interaction with the complex geographical features inside the bay were considered as insignificant on storm surge response. A part of such simplifications was justified by partitioning off the entire study area into three regions, within which the assumption of the slowly varying geographical feature is applicable. However, in order to make wide use of SRF methodology and improve the credibility in the predictions from SRF, research to account for the listed variability in the hurricane meteorology and the regional geography has to be conducted. Additionally, the prediction made by SRF was unaffected by the other forcing factors, such as wave radiation and astronomical tide. Therefore, for real world application, the hurricane impact should be evaluated after coupling with the listed other forcing factors by utilizing the SRF surge prediction as an initial estimation. Finally, in order to apply the SRF method for the storm surge hazard analysis, further incorporation with the statistical application has to be made.

REFERENCES

Aldama, A., Aguilar, A., Kolar, R., and Westerink, J.J. (2000). "A mass conservation analysis of the GWCE formulation." *Computational Methods in Water Resources*, 2, 907-912.

Borgman, L. E., Miller M., Butler L., and Reinhard R. (1992). "Empirical simulation of future hurricane storm histories as a tool in engineering and economic analysis." *Proceedings of 5th International conference of Civil Engineering in the Ocean*, College Station, TX, 42-65.

Cardone, V.J., Greenwood, C. V., and Greenwood, J.A. (1992). "Unified program for the specification of hurricane boundary layer winds over surfaces of specified roughness." *Contract Report CERC-92-1*, US Army Corps of Engineers, Vicksburg, MS.

Chow, S. H. (1971). "A study of the wind field in the planetary boundary layer of a moving tropical cyclone," M.S. Thesis, New York University, New York.

Collins, E. (2006). "One year later: the repair/rebuild efforts following Hurricane Katrina." *GoStructural.com*, Online article. http://www.gostructural.com/article.asp?id=1092

Dean, R. G., and Dalrymple, R. A. (1984). "Water wave mechanics for engineers and scientist." *Advanced Series on Ocean Engineering*, 2,157-159.

Douglass, S. L., Lindstrom, J., Richards, J.M., and Shaw, J.(2005). "An estimate of the extent of U.S. coastal highways." Presentation to Transportation Research Board,

Hydraulics, Hydrology, and Water Quality Committee Meeting, Washington DC, Online. http://www.southalabama.edu/usacterrec/chighwayestimate.pdf

Google satellite images (2009a). "Locations of twenty target bridges along Texas coast (red dots)." 1 May. 2009. http://earth.google.com.

Google satellite images (2009b). "Bridges (the red circles) near the eastern boundary of the Texas coast." 11 Feb. 2009, http://earth.google.com.

Google satellite images (2009c). "A bridge (the red circle) at Rollover Pass in Galveston." 11 Feb. 2009, http://earth.google.com.

Google satellite images (2009d). "Bridges (the red circles) near the entrance of Galveston Bay" 11 Feb. 2009, http://earth.google.com.

Google satellite images (2009e). "Bridges (the red circles) of FM 2004 Road (top), and San Luis Pass (bottom) in Galveston." 11 Feb. 2009, http://earth.google.com.

Google satellite images (2009f). "Bridges (the red circles) on FM1495 Road (left) and Hwy 332 (right) near Freeport." 11 Feb. 2009, http://earth.google.com.

Google satellite images (2009g). "Bridges (the red circles) along Highway 35 in Matagorda Bay." 11 Feb. 2009, http://earth.google.com.

Google satellite images (2009h). "A Bridge (the red circles) on Lyndon B. Johnson Causeway in Aransas." 11 Feb. 2009, http://earth.google.com.

Google satellite images (2009i). "Bridges in Corpus Christi." 11 Feb. 2009, http://earth.google.com.

Google satellite images (2009j). “Location (marked by maroon dots) of two damaged bridges in Galveston during Hurricane Ike.” 1 May. 2009, http://earth.google.com.

Gray, W. G. (1982). "Some inadequacies of finite element models." *Adv. Water Resources,* 5(September), 171-177.

Gulf Coast Information System (GCIS, 2006). "Highway 90 bridge damage." Hurricane Katrina damage photos - Mississippi Gulf Coast, Online photos, http://www.gulf-coast.com/Katrina-Information/Katrina-Pictures/HurricaneKatrinaPictures-2.html

Gumbel, E. J. (1959). “Statistics of Extremes.” Oxford University Press, London, 1959

Ho, F.P. and Myers, V.A. (1975). “Joint Probability Method of Tide Frequency Anaylsis applied to Apalachicola Bay and St. George Sound, Florida.” *NOAA Technical Report NWS18*, Silver Spring, MD

Holland, G. J. (1980). "An analytic model of the wind and pressure profiles in hurricanes." *Monthly Weather Review*, 108(80), 1212-1218.

Irish, J. L., and Cañizares, R., (2009). "Storm-wave flow through tidal inlets and its influence on bay flooding." *J. Waterways Port, Coasta and Ocean Eng.,* 135(2), 52-60.

Irish, J.L., and Resio, D.T. (2009) "A hydrodynamics-based surge scale for hurricanes." *Ocean Eng*., in press.

Irish, J. L., Resio, D. T., and Cialone, M. A. (2009). " A surge response function approach to coastal hazard assessment—Part 2: quantification of spatial attributes of response functions." *Nat Hazards,* doi: 10.1007/s11069-009-9381-4

Irish, J. L., Resio, D. T., and Ratcliff, J. J. (2008). "The influence of storm size on hurricane surge." *J. Phys. Oceanogr.*, 38(9), 2003-2013.

Jin, J. (2008). "Rollover Pass and Pelican Island Bridge." Digital camera images, Assistant Professor, Maritime Systems Engineering, Texas A&M University - Galveston.

Jones, L. (2009, March 19). "Pelican Island Bridge repair work stuck between agencies." *The Daily News*, Galveston. Online. http://galvestondailynews.com/story.lasso?ewcd=7d25b30b4537fa83

Kinmark, I. P. E. and Gray, W. G. (1984). "The 2Δx-test: A tool for analyzing spurious oscillations." *Adv. Water Resources*, 8 (September), 129-135.

Kolar, R.L. and Westerink, J.J. (2000). "A look back at 20 years of GWC-based shallow water models." *Computational Methods in Water Resources* 2(8), 899-906

Luettich, R.A., Westerink, J. J., and Scheffner, N.W.(1991) "ADCIRC: An advanced three-dimensional circulation model for shelves, coasts, and estuaries: Report 1: theory and methodology of ADCIRC-2DDI and ADCIRC-3DL", *Technical Report DRP-92-6*, US Army Corps of Engineers, Washington, DC.

Lynch, D. R. (1983). "Progress in hydrodynamic modeling review of U.S. contributions, 1979-1982." *Rev. Geophys, Space Phys*, 21(3), 741-754.

Lynch, D. R. and Gray W. G. (1979). "A wave equation model for finite element tidal computations." *Comput. Fluids* 7, 207–228

National Weather Service (2008). "Hurricane IKE advisory archive: Advisory 48 ", National Hurricane Center. Online. http://www.nhc.noaa.gov/archive/2008/

IKE.shtml

Navon, I. M. (1988). " A review of finite-element methods for solving the shallow-water equations." *Computer Modeling in Ocean Engineering*, 273-278.

Niedoroda, A.W., Resio, D., Toro G., Divoky D., Das H., and Reed C. (2007). "Evaluation of the storm surge hazard in coastal Mississippi." *Proceedings of 10th International Workshop on Wave Hindcasting and Forecasting and Coastal Hazards, 2007*, Oahu, HI.

Niedoroda A.W., Resio, D., Toro, G., Divoky, D., and Reed, C. (2008) "Efficient strategies for the joint probability evaluation of storm surge hazards." *Proceedings of Solution to Coastal Disasters Congress 2008*, 242-255.

NOAA (2009 June 1) "Hurricane Carla." Hurricane history. Online. http://www.srh.noaa.gov/crp/docs/research/hurrhistory/Carla/carla.html.

NOAA (1982) "Pertinent meteorological and hurricane tide data for Hurricane Carl." *Technical Report NWS32*, Silver Spring, MD

Padgett, J., Roches, R. D., Nielson, B., Yashinsky, M., Kwon, O.S., Burdette, N., and Tavera, E. (2008). "Bridge damage and repair costs from Hurricane Katrina." *Jounal of Bridge Engineering* 13(1), 6-14.

Powell, M.D. and Reinhold, T. A.(2007). "Tropical cyclone destructive potential by integrated kinetic energy." *Bull. Amer. Meteor. Soc.*, 88, 513-526.

Public Information Office of Texas Department of Transportation (2008). "TxDOT Responds to Hurricane Ike." Houston, Texas, online at Newsrouter.com. http://www.newsrouter.com/NewsRouter_Uploads/67/TexDOT.pdf.

Rappleye, C. (2008, October 8). "Repairs to start on Rollover Pass Bridge." *Beaumont Enterprise.* Online. http://www.beaumontenterprise.com/news/local/repairs_to_start_on_rollover_pass_bridge_10-08-2008.html

Resio, D. T., Irish, L. J., and Cialone, M. (2009). "A surge response function approach to coastal hazard assessment. Part 1: Basic concepts." *Nat. Hazards*, 2009, doi: 10.1007/s11069-009-9379-y

Resio D.T. and Westerink, J. J. (2008). "Modeling the physics of storm surges." *Physics Today*, 61(99), 33.

Scheffner, N., Borgman, L. and Mark, D. (1996). "Empirical simulation technique applications to a tropical storm surge frequency analysis of the coast of Delaware." *Journal of waterway, prot, coastal, and ocean engineering*, 122(2).

Thompson, E. F., and Cardone, V.J. (1996). "Practical modeling of hurricane surface wind fields." *Journal of Waterways, Port, Coastal, and Ocean Engineering*, July/August 1996, 198-205.

Tonkin, H., Holland, G.J., Holbrook, J., and Henderson-Sellers, A. (2000). "An evaluation of thermodynamic estimates of climatological maximum potential tropical cyclone intensity." *Monthly Weather Review*, 128(March 2000), 746-762

UN Atlas of the Oceans (USES 2000). "Human settlements on the coast." *USES. Online.* http://www.oceansatlas.org/servlet/CDSServlet?status=ND10b3Bkb3duJjY9ZW4mMzM9KiYzNz1rb3M~.

U.S. Department of Commerce (1979). “Meteorological criteria for standard project hurricane and probable maximum hurricane wind fields, Gulf and East Coasts of the United States.”, *NOAA Tech Rep NWS 23*, Washington, DC

U.S. Department of Commerce (1972). “Memorandum HUR-7-120, Revised standard project hurricane criteria for the Atlantic and Gulf Coasts of the United States.” *National Hurricane Research Project HUR-7-120*, New Orleans.

U.S. Department of Commerce (1959). “Meteorological consideration pertinent to standard project hurricane, Atlantic and Gulf Coasts of the United States.” *National Hurricane Research Project Rep. 33*, Washington, DC

USGS(2008) “Monitoring inland storm surge and flooding from Hurricane Ike in Texas and Louisiana, September 2008”, *U.S. Geological Survey Open-File Report 2008–1365*, Online. http://pubs.usgs.gov/of/2008/1365.

USGS (2005). "Hurricane Rita surge data, southwestern Louisiana and southeastern Texas, September to November 2005." *Data Series 220*, Reston, VA.

Westerink, J.J., Luettich, R. A., Feyen, J.C., Atkinson, J.H., Dawson, C., Roberts, H.J., Powell, M.D., Dunion, J.P., Kubatko, E.J., and Pourtaheri, H. (2008). "A basin- to channel-scale unstructured grid hurricane storm surge model applied to southern Louisiana." *Monthly Weather Review*, 136, March 2008, 833-864.

Westerink J.J., Luettich, R. A., and Scheffner N.W. (1994). "ADCIRC: An advanced three-dimensional circulation model for shelves, coasts, and estuaries: Report 4: Hurricane strom surge modeling using large domains." *Technical Report DRP-92-6*, US Army Corps of Engineers, Washington, DC.

Westerink, J.J., Luettich, R. A., Baptista, A. M., Scheffner, N.W., and Farrar, P. (1992). "Tide and storm surge perdictions using finite element model." *Journal of Hydraulic Engineering*, 118(10), 1373-1390.

Westerink, J. J., Muccino, J. C., and Luettich, R. A. (1991). "Tide and storm surge computations for the Western North Atlantic and Gulf of Mexico." *Esturine and coastal modeling*, 538-550.

Westerink, J. J. and Gray, W. G. (1991). "Progress in surface water modeling." *Reviews of Geophysics*, 29, 210-217.

APPENDIX A

SURGE RESPONSE FUNCTION DEFINED NEAR 17 TEXAS COASTAL BRIDGES

Table 9. Locations of the 17 selected coastal bridges

Bridge No.	Stn. No.	Description	Lon.	Lat	Location
1	45	State Hwy Park Road 22_No.1	-97.214	27.619	Corpus Christi
2	47	State Hwy Park Road 22_No.2	-97.240	27.635	
3	48	Kennedy Causeway	-97.261	27.658	
4	51	Padre Island Bridge	-97.312	27.680	
5	53	Nueces Bay Causeway 1	-97.395	27.813	
6	55	Nueces Bay Causeway 2	-97.370	27.844	
8	65	Johnson Causeway	-97.020	28.120	
9	84	Port Lavaca	-96.598	28.650	Matagorda
10	88	Weedhaven	-96.432	28.732	
11	116	FM1495 Road	-95.341	28.922	Galveston
12	117	Hwy 332	-95.293	28.956	
14	130	FM 2004 Road	-95.207	29.213	
16	142	Pelican Island Bridge	-94.824	29.311	
17	147	Texas City Dike Road	-94.810	29.363	
19	181	Martin Luther King Jr. Drive (Hwy 82)	-93.895	29.766	
20	182	Jetty Road	-93.853	29.696	

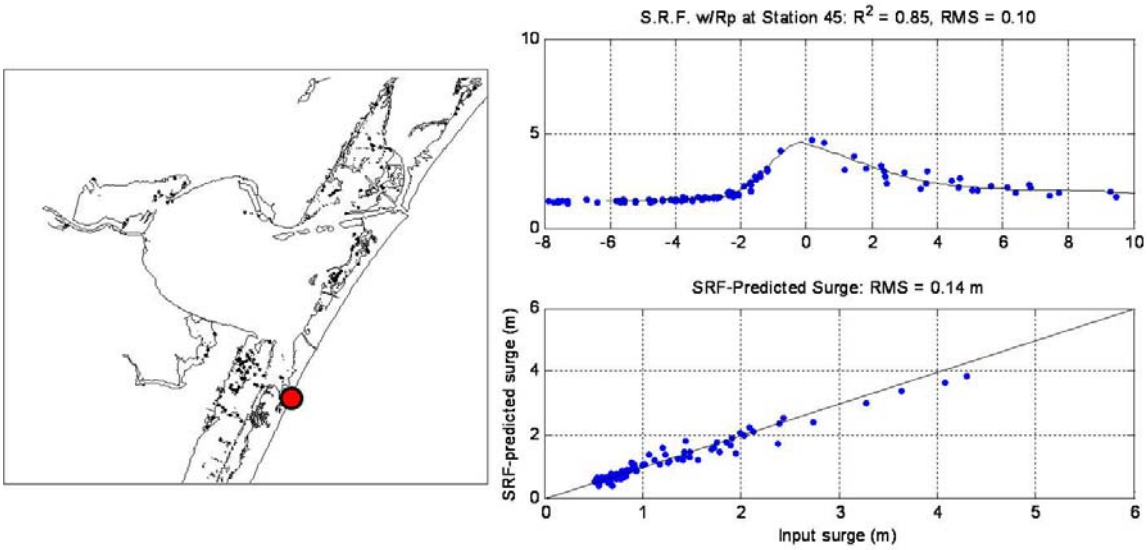

A- 1 A surge response function developed at the bridge No. 1. State Hwy Park Road 22 in Corpus Christi.

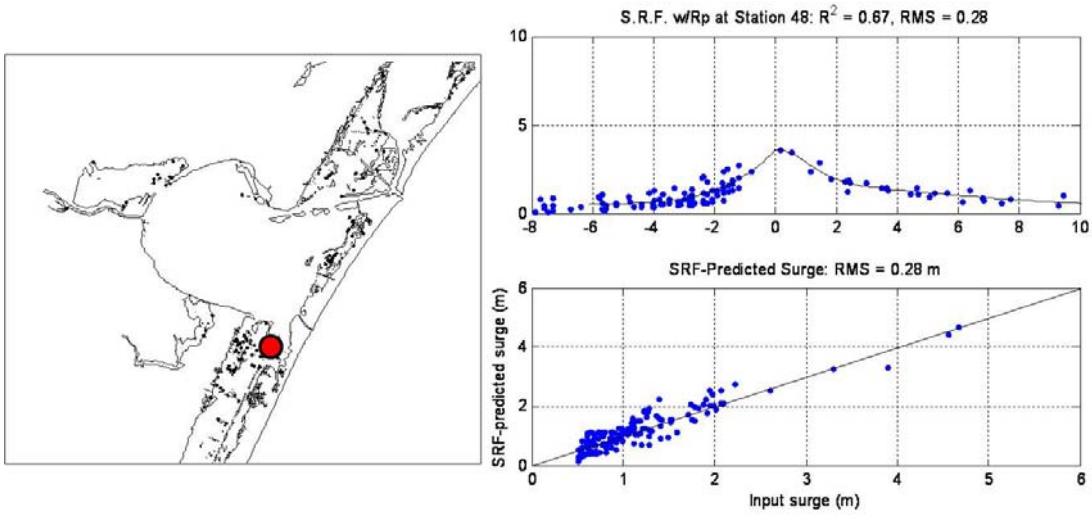

A- 2 A surge response function developed at the bridge No. 2. State Hwy Park Road 22 i n Corpus Christi.

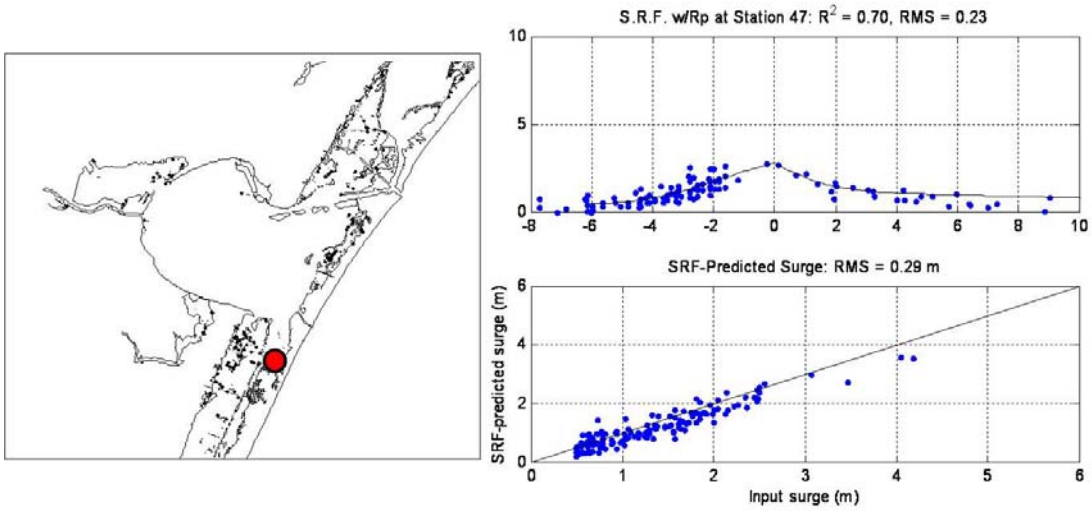

A- 3 A surge response function developed at the bridge No.3 along the Kennedy Causeway in Corpus Christi.

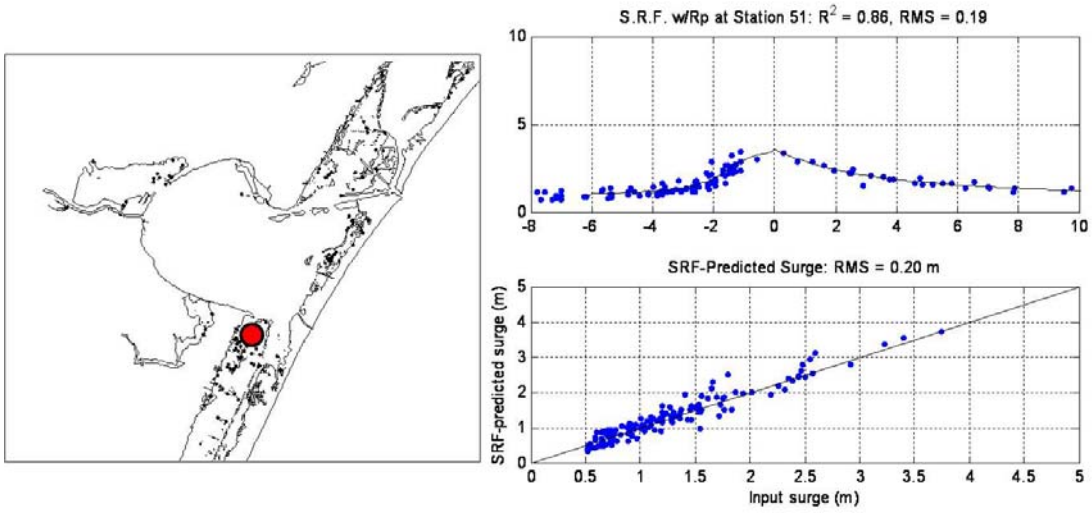

A- 4 A surge response function developed at the bridge No.4. Padre Island Bridge in Corpus Christi.

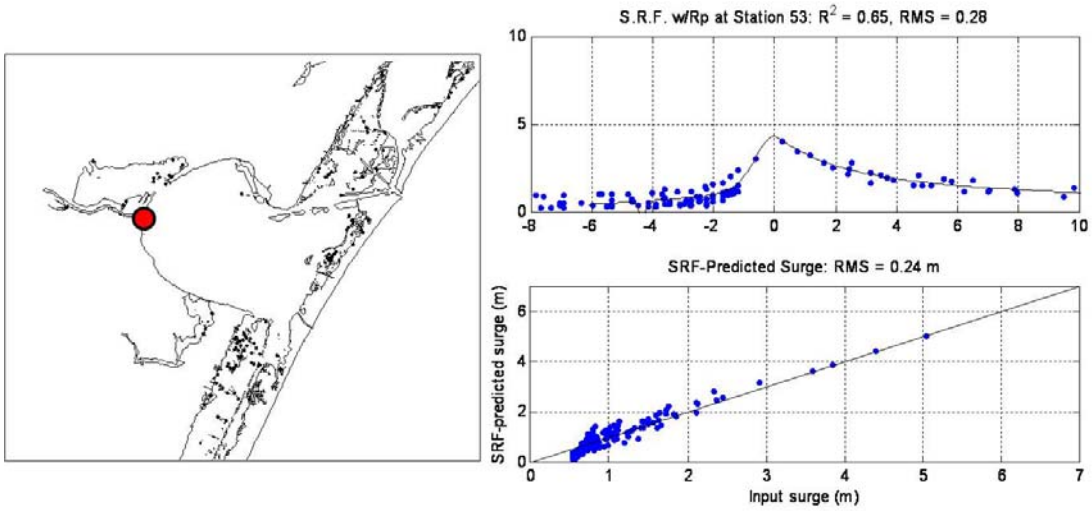

A- 5 **A surge response function developed at the b**ridge No. 5 along the Nueces Bay Causeway in Corpus Christi.

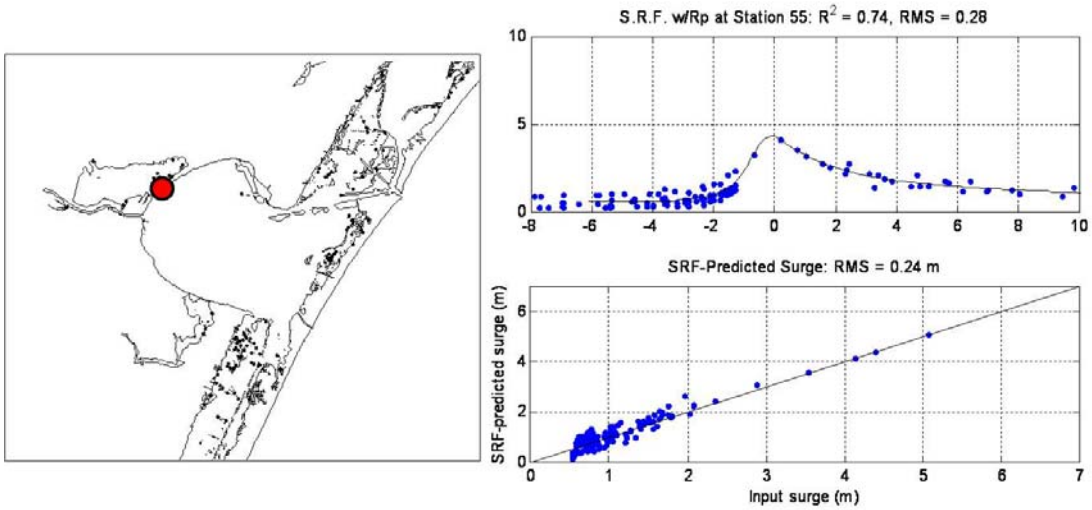

A- 6 A surge response function developed at the bridge No. 6 along the Nueces Bay Causeway in Corpus Christi.

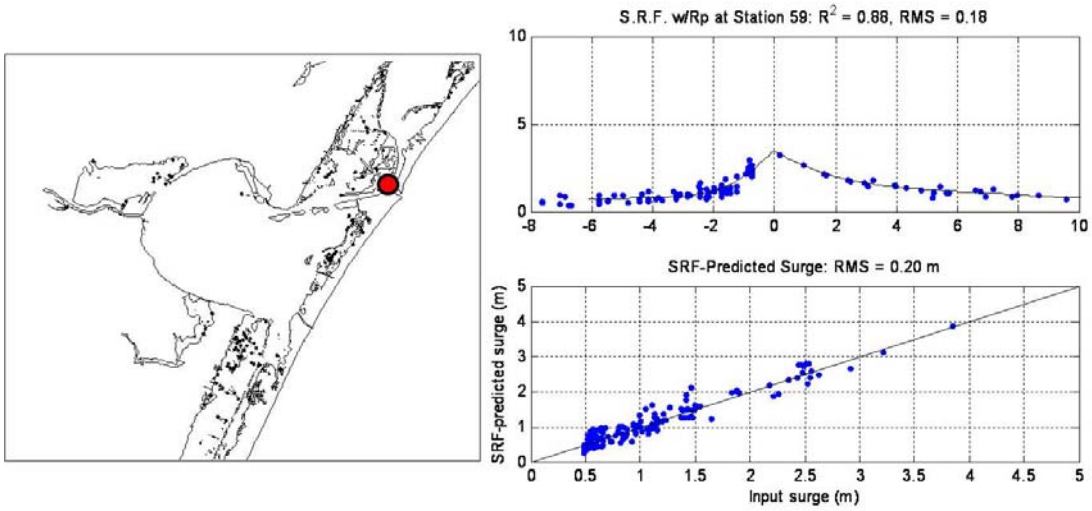

A- 7 A surge response function developed at the bridge No. 7 along the Cemetery Road near Corpus Christi.

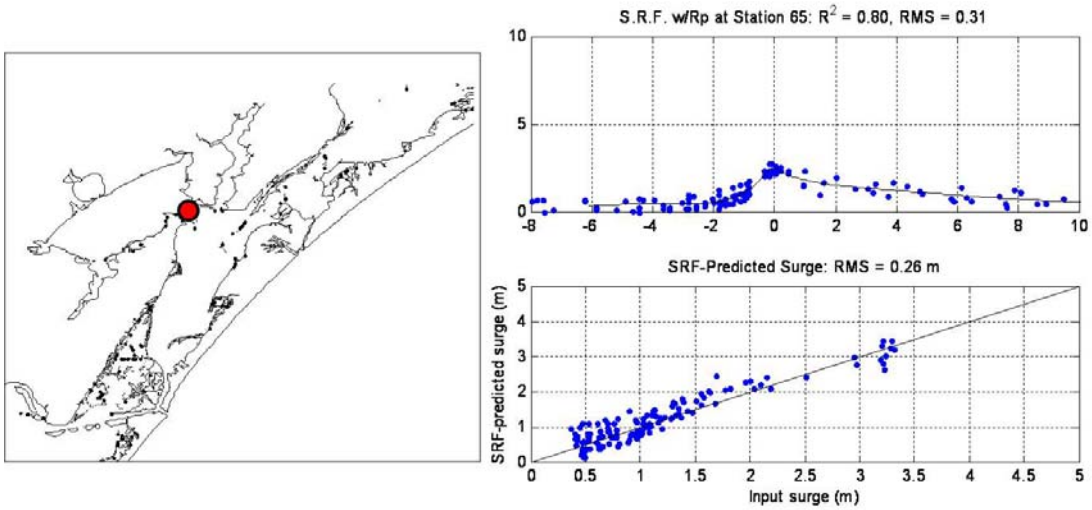

A- 8 A surge response function developed at the bridge No. 8 along the Johnson Causeway near Corpus Christi.

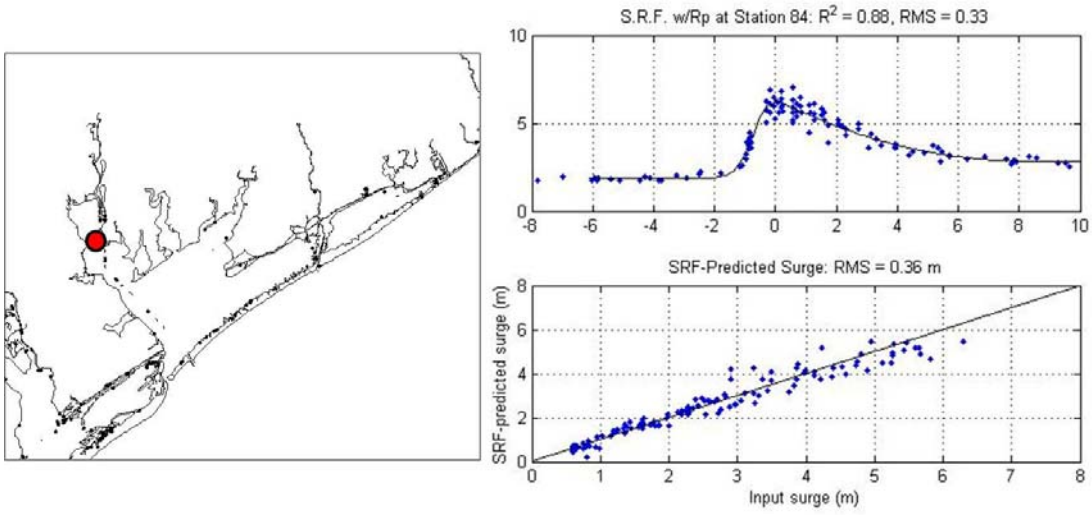

A- 9 A surge response function developed at the bridge No. 9. Port Lavaca in Matagorda Bay.

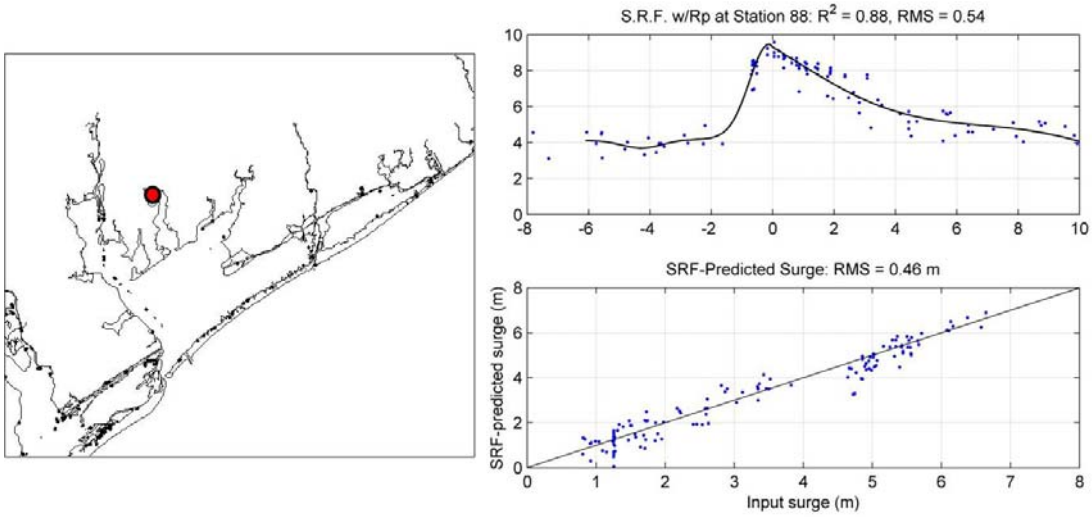

A- 10 A surge response function developed at the bridge No. 10 near Weedhaven in Matagorda Bay.

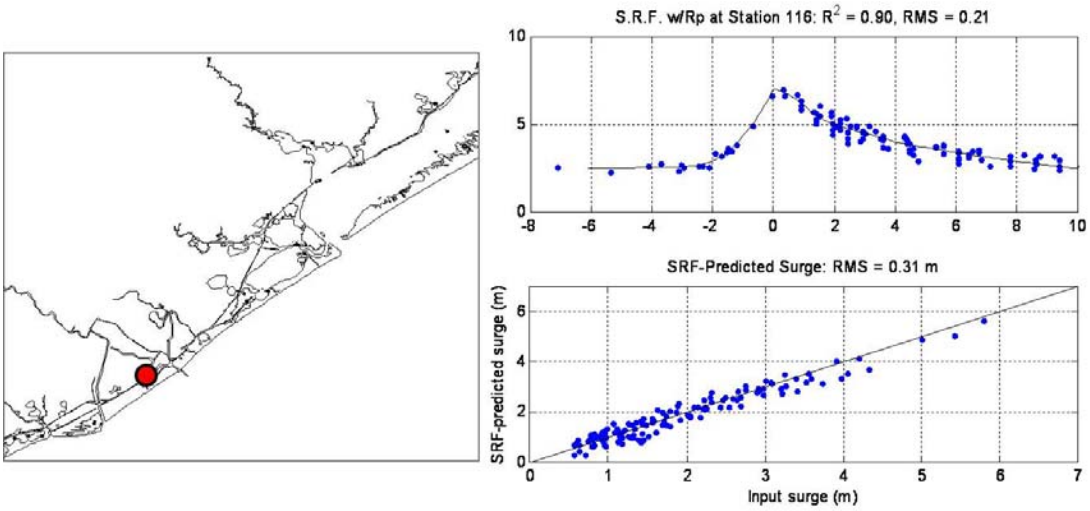

A- 11 A surge response function developed at the bridge No. 11 along the FM1495 Road in Galveston.

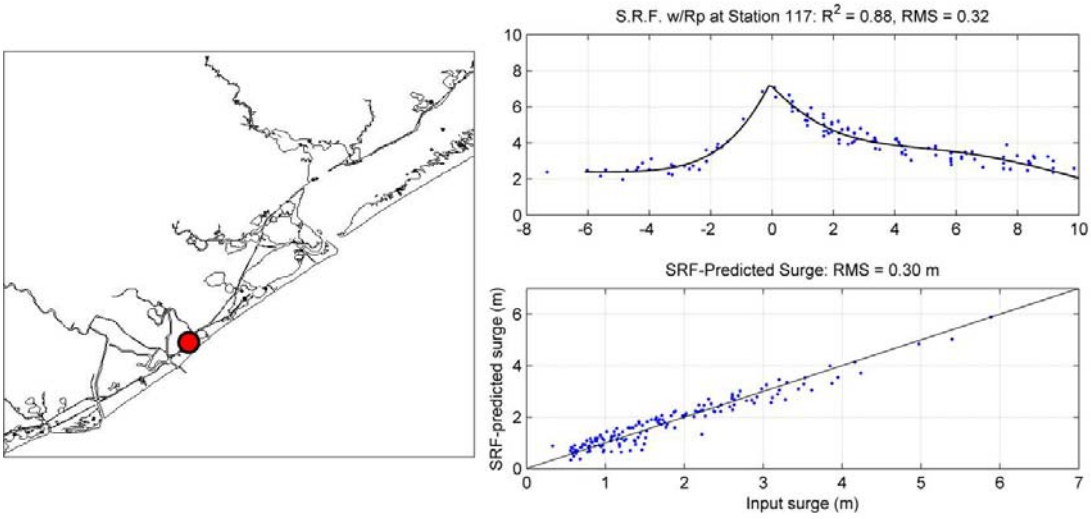

A- 12 A surge response function developed at the bridge No. 12 along the Hwy 332 in Galveston.

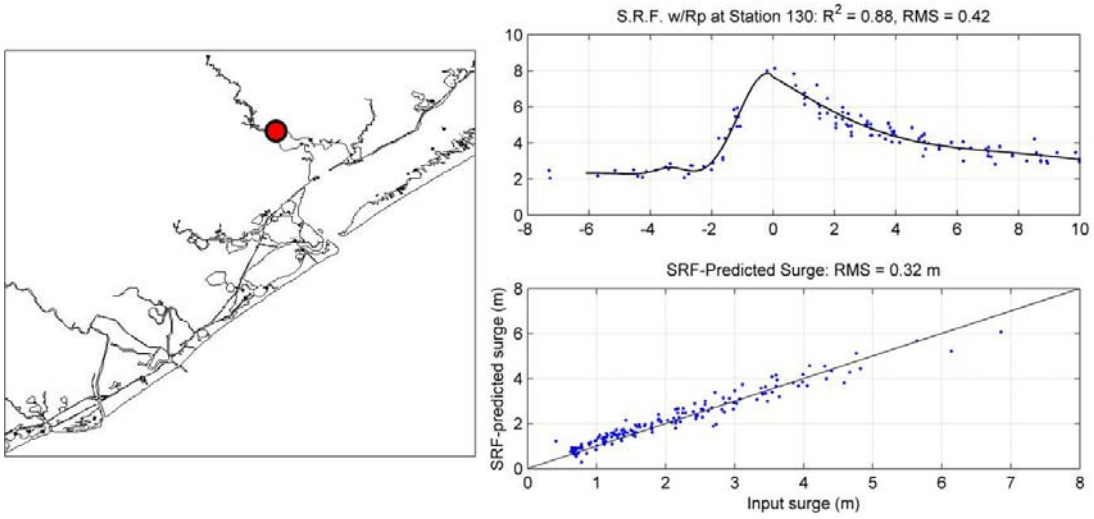

A- 13 A surge response function developed at the bridge No. 14. FM 2004 Road in Galveston.

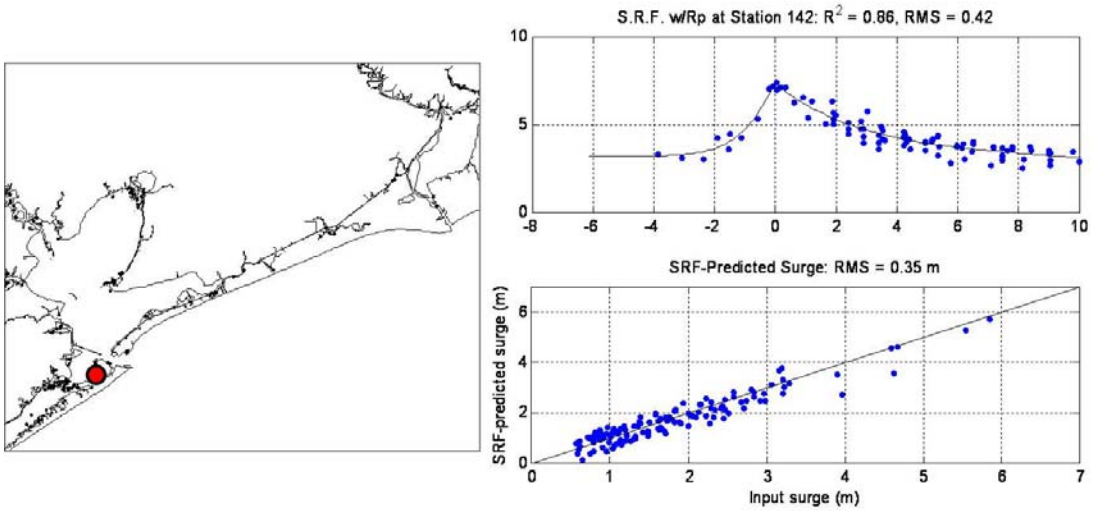

A- 14 A surge response function developed at the bridge No. 16. Pelican Island Bridge in Galveston.

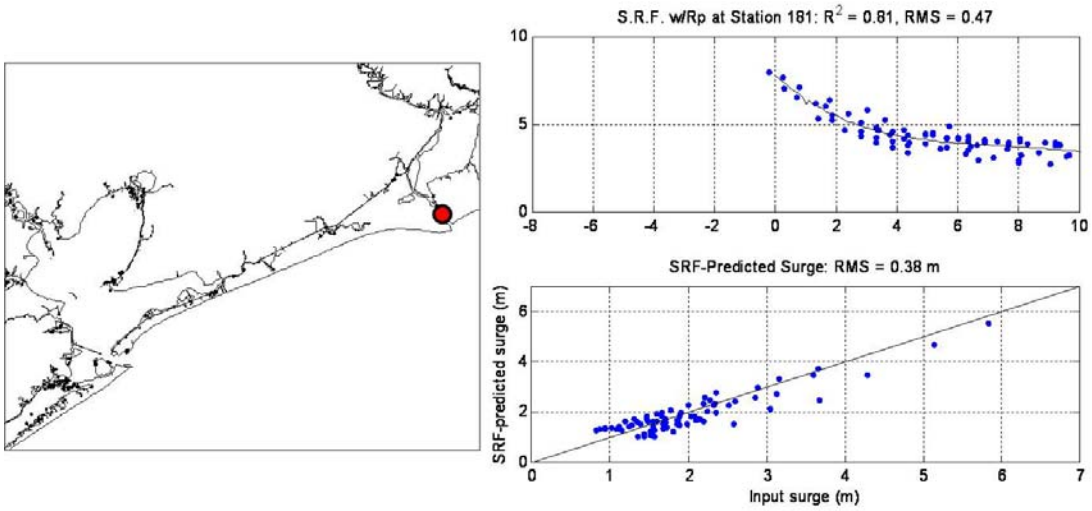

A- 15 A surge response function developed at the bridge No. 19. Martin Luther King Jr. Drive (Hwy 82) in Galveston.

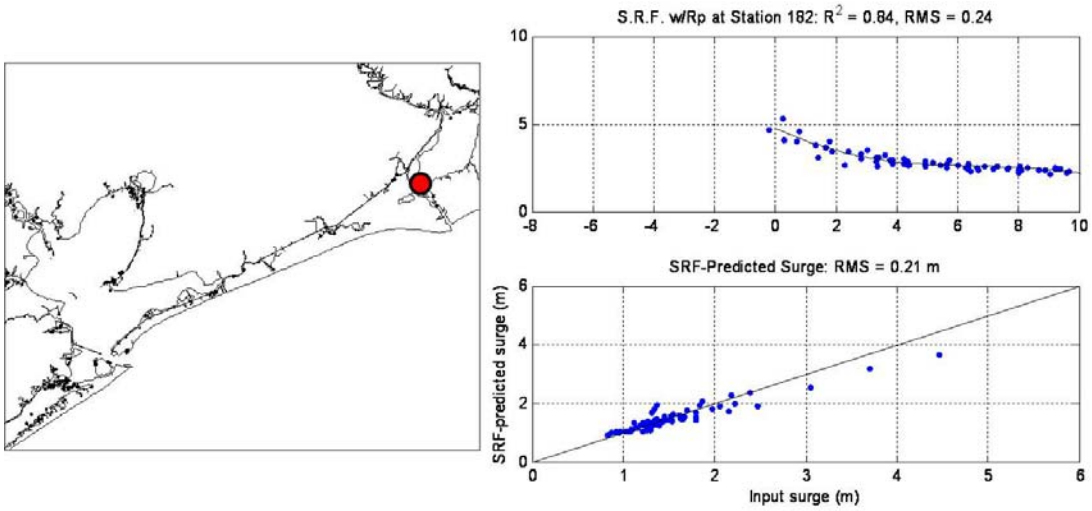

A- 16 A surge response function developed at the bridge No. 20. Jetty Road in Galveston.

VITA

Name: Youn Kyung Song

Email Address: songakty@yahoo.com

Education: B.S., Civil Engineering, Han Yang University, 2007

M.S., Civil Engineering, Texas A&M University, 2009

Mailing Address: 3136 TAMU, College Station, TX 77843-3136